FEMTOSECOND LASER MICROMACHINING

FEMTOSECOND LASER ABLATION
OF
SELECTED DIELECTRICS AND METALS

By
QIANG LIU, B.Sc.

A Thesis
Submitted to the School of Graduate Studies
in Partial Fullment of the Requirements
For the Degree
Master of Engineering

McMaster University
©Copyright by Qiang Liu, September 2001

MASTER OF ENGINEERING (2001)
(Engineering Physics)

McMaster University
Hamilton, Ontario

TITLE: FEMTOSECOND LASER ABLATION OF SELECTED DIELECTRICS AND METALS.

AUTHOR: Qiang Liu, B.Sc. (Harbin Institute of Technology)

SURPERVISOR: Professor H. Haugen

NUMBER OF PAGES: lxviii, 68

ABSTRACT

Ti: sapphire femtosecond laser ablation of dielectrics (fused silica and BK7 glass) and metals (Cu, Fe, Al) is presented. Results of laser -induced breakdown experiments in fused silica and BK7 glass employing 130 fs –1.7 ps, 790 nm laser pulses are reported. The fluence ablation threshold does not follow the scaling of $\phi_{th} \sim \tau^{1/2}$ when pulses are shorter than 1 ps. Single-shot and multi-shot (130 fs pulse) ablation of selected materials are investigated with laser wavelengths of 395 nm, 790 nm, and 1300 nm. The ablation threshold is almost independent of the laser wavelength. The surface morphologies in metals after ultrashort pulse ablation are very different from dielectrics and semiconductors. The roughness of the ablated surface depends on the thermal properties of the metal target. The preliminary TEM result from Cu single crystal that was irradiated by single laser pulses shows few defects in the center region of the ablated crater. Single-shot ablation of single-crystal Fe induces much different surface features than on selected samples of poly-crystal Fe metal.

ACKNOWLEDGMENTS

I wish to express my sincere appreciation to my supervisor, Dr. Harold Haugen for his support, direction, and advice during the course of my graduate studies. I would like to thank Dr. George Weatherly for expertise on electron microscopy analysis and materials expertise. I would also like to thank these persons in BIMR for their help: Andy Duft for his guidance and instruction in sample preparation, material processing, and AFM analysis; Junji Yamanaka for the TEM analysis; Gim Garrett for his metal samples; Guanglei Liu for the SEM training; Chris Butcher for the polishing training; and Fred Pearson for his advice and instruction on material processing. I would also like to thank Dr. Marek Niewczas for his copper samples and knowledge on crystalline materials.

A very special thanks goes out to Andrzej Borowiec. The work presented in this thesis could not have proceeded without his help and continuing support. I also want to thank Henry Tiedje, Tim Lampman, Michael Brennan and Joel Milgram for their assistance. It is a nice memory to have been working with these people.

Finally, I am very grateful to my wife Jing Wu and to my parents for their love, encouragement and support.

TABLE OF CONTENTS

CHAPTER 1. INTRODUCTION 1

1.1 INTRODUCTION 1

1.2 THESIS OUTLINE 1

CHAPTER 2. FUNDAMENTALS OF LASER MICRO-FABRICATION 3

2.1 TECHNIQUES FOR MICROMACHINING 3

2.1.1 Chemical Etching 4

2.1.2 Electron/Ion Beam Etching 4

2.1.3 X-ray Lithography 5

2.2 INTRODUCTION TO LASER MICROMACHINING 6

2.3 MATERIALS PROCESSING WITH LASERS 7

2.4 ULTRAFAST LASER MICROMACHINING 10

CHAPTER 3. ULTRASHORT PULSE LASERS 14

3.1 INTRODUCTION 14

3.2 GROUP VELOCITY DISPERSION AND DISPERSION COMPENSATION 16

3.3 CHIRPED PULSE AMPLIFICATION IN ULTRASHORT PULSE LASERS 18

3.4 TIME DOMAIN MEASUREMENT OF FEMTOSECOND LASER PULSES 20

CHAPTER 4. FEMTOSECOND LASER ABLATION OF DIELECTRICS 23

4.1 INTRODUCTION 23

4.2 MOTIVATIONS AND BACKGROUND 24

4.3 EXPERIMENTAL 27

4.4 SINGLE-SHOT RESULTS AND DISCUSSION 29

4.5 MULTI-SHOT RESULTS 38

4.6 POTENTIAL APPLICATIONS 43

4.6.1 Biochemical Sample Holder *43*

4.6.2 Photonics Components Processing *45*

CHAPTER 5. FEMTOSECOND LASER ABLATION OF METALS 48

5.1 INTRODUCTION 48

5.2 EXPERIMENTAL 51

5.3 SINGLE-SHOT RESULTS AND DISCUSSION 52

5.4 SINGLE-SHOT ABLATION OF POLY-CRYSTAL FE AND SINGLE-CRYSTAL FE 58

5.5 POTENTIAL APPLICATIONS 60

CHAPTER 6. CONCLUSION 61

REFERENCES: 64

TABLE OF FIGURES

Figure 2.1: Traditional semiconductor chemical processing 4

Figure 2.2: Schematic view of electron beam projection system 5

Figure 2.3: Diagram of long pulse laser ablation of material (Figure adapted from "Tutorial on laser micromachining", Potomac Laser Micro Tools, Inc) 8

Figure 2.4: Ultrafast laser ablation of material (Figure adapted from "Micromachining handbook", Clark-MXR, Inc) 11

Figure 2.5: Diagram of multi-photon absorption 13

Figure 3.1: Kerr lens mode locking 15

Figure 3.2: Dispersion compensation with prism pair 17

Figure 3.3: Diagram of CPA (Figure adapted from the CLEO 2001 short course "Fundamental of ultrashort pulse amplification", C. P. J. Barty, Lawrence Livermore National Lab) 18

Figure 3.4 (a): Stretcher 19

Figure 3.5 (b): Compressor 20

Figure 3.6: Diagram of autocorrelation and measurement result of a 130 fs pulse 22

Figure 4.1: (left) Cracks in fused quartz induced by five nanosecond laser pulses (λ=351 nm, τ=138 ns with fluence ~314 J/cm^2), (right) crater in fused quartz made by five femtosecond laser pulses (λ=790 nm, τ=130 fs with fluence ~1.5 J/cm^2), no cracks 24

Figure 4.2: Micromachining setup (Figure provided by A. Borowiec) 28

Figure 4.3: (left) 395 nm (from doubling frequency of 790 nm laser) laser beam shape focused by a 10× objective; (right) 790 nm laser beam shape focused by a 10× objective 29

Figure 4.4 (a): SEM image of the fused silica single-shot ablated at different fluence (from 5.1 J/cm^2 to 0.64 J/cm^2) by single laser pulse (τ=130 fs, λ=790 nm) 30

Figure 4.4 (b): Zoom view of the crater #1 which is made with a laser fluence of 5.1 J/cm^2 30

Figure 4.4 (c): Zoom view of the crater #10 which is made with a laser fluence of 0.64 J/cm^2 30

Figure 4.5: Squared diameter D^2 of the ablated craters in BK7 (left) and fused silica (right) as a function of the laser fluence ϕ_o (λ=780 nm, τ=130 fs) 31

Figure 4.6: Single-shot ablation threshold of fused silica (left) and BK7 glass (right) with ultrashort pulses of different laser durations (from 130 fs to 1000 fs) 32

Figure 4.7: BK7 glass (left) and fused silica (right) ablation threshold with different laser wavelengths 34

Figure 4.8 (a): (left) Fused silica with 395 nm at fluence 5.8 J/ cm2, (right) BK7 glass with 395 nm at fluence 2.8 J/cm^2 35

Figure 4.8 (b): Laser ablation of fused silica (left) and BK7 glass (right) at 790 nm with a laser fluence 6.62 J/cm^2 35

Figure 4.9: SEM images of fused silica surface ablated by single laser pulse (λ=780 nm, τ=130 fs) with energy from 150 μJ/pulse in the first line (top) to 30 μJ/pulse in the last line (bottom), laser focusing was moved down 20 μm in each step in each row (from left to right) 37

Figure 4.10 (a): Gaussian beam shape focused by gradient index lens 37

Figure 4.10 (b): Crater sizes in first line of Figure 4.9 with different focusing position.. 37

Figure 4.10 (c): Fitting the crater diameters to a Gaussian beam 38

Figure 4.11: Multi-shot pattern in fused silica with laser (τ=130 fs and λ=790 nm) pulse number N=1 (top) to 10 (bottom) at different fluences from high 13.5 J/cm^2 (right) to near threshold fluence 1.35 J/cm^2 (left) 39

Figure 4.12 (a): Laser ablation in zinc titania glass with laser (τ=130 fs and λ=790 nm) pulse number N=1 (left) and N =2 (right).. 40

Figure 4.12 (b): Laser ablation in zinc titania glass with laser (τ=130 fs and λ=790 nm) pulse number N=3 (left) and N=4 (right).. 41

Figure 4.13 (a): Multi-shot pattern in fused silica at laser duration 1700 fs with laser (λ=790 nm) pulse number N=1 (top) to 10 (bottom) with step-attenuated fluence from right side to left 41

Figure 4.13 (b): Multi-shot pattern in fused silica at laser duration 130 fs with laser pulse (τ=130 fs and λ=790 nm) number N=1 (top) to 10 (bottom) with step-attenuated fluence from right side to left.. 42

Figure 4.14: (left) Biochemical sample is held in a smooth crater, (right) crater array fabricated in fused silica working as biochemical holder 44

Figure 4.15: Ti: sapphire laser cutting trench (left) and gratings (right) in dielectrics..... 46

Figure 5.1: Single-shot irradiation of semiconductors (Si, GaAs, and InP) (SEM images from A. Borowiec) and metals (Cu, Al, and Fe) at specified laser fluences at a wavelength of 790 nm 51

Figure 5.2: Squared diameters D^2 of the ablated craters in Cu (left) and Fe (right) with single laser pulse (τ=130 fs, λ=790 nm and 395 nm) as a function of the laser fluence 53

Figure 5.3: AFM images of single-shot irradiation of Cu single-crystal with fluence 1.7 J/cm^2 (upper-left) and 0.86 J/cm^2 (upper-right), and (below) the profile of the crater ablated with laser fluence 1.7 J/cm^2........ 55

Figure 5.4: TEM observations of Cu single crystal after 5 μJ single pulse laser irradiation. (a): TEM image of laser irradiated Cu single crystal after ion milling. This area is located in the central part of the laser-produced crater. The arrow shows the position, which corresponds to the following micrograph, for detailed observation. (b): Bright field image around the boundaries. The arrows show the position of grain boundary and sub- boundary. (c): Selected area electron diffraction pattern corresponding to the region A in the bright field image (b). (d): Selected area electron diffraction pattern corresponding to the region B in the bright field image (b) (TEM images provided by Junji Yamanaka) 57

Figure 5.5 (a): Fe single-crystal single-shot ablation with high (113 J/cm^2) and medium (3.5 J/cm^2) fluence 58

Figure 5.5 (b): Poly-crystal Fe single-shot ablation with medium fluence (4.3 J/cm^2) and low fluence (0.54 J/cm^2) 59

Figure 5.6: Squared diameter D^2 of the ablated craters in single-crystal Fe (left) and poly-crystal Fe (right) with single laser pulse (τ=130 fs, λ=790 nm) as a function of the laser fluence 59

Figure 5.7: (left) Gratings in TiAl , (right) highly reproducible craters array in Fe........ 60

Chapter 1. Introduction

1.1 Introduction

The rapid advances in the generation and amplification of ultrashort laser pulses (<1 pico-second) have opened up many new possibilities in laser-matter interactions and materials processing. The extreme short pulse width also makes it easy to achieve very high peak laser intensity with low pulse energy. For example, a laser pulse with a pulse-width of 100 femto-seconds (10^{-13} s) and pulse energy of only one-third of 1 mJ has a peak intensity of 10^{15} W/cm^2 when focused to a 20 μm-diameter spot. A 10-nanosecond-long laser pulse would have to have 100 J in the pulse to reach the same intensity. In such a high intensity with an ultrashort pulse laser, no materials can withstand the electric field. This means that with an ultrashort laser pulse we can machine very hard materials as well as materials with very high melting points such as diamond, fused silica, etc. Also, people can focus the ultrashort pulse inside transparent materials to induce damage at a sub-surface level via nonlinear interaction. At the same time, the laser pulse is so short that the energy hardly has the time to diffuse away when machining high thermal conductivity materials such as Cu and Al, and the efficiency of the machining process is high.

1.2 Thesis Outline

This thesis presents the ultrashort pulse laser ablation of dielectrics and metals. The second chapter will provide the necessary background in materials micro-processing and

laser ablation. Chapter three contains an overview of ultrashort pulse lasers. Experimental results and discussion of ultrashort pulse laser ablation of dielectrics and metals are outlined in chapters four and five respectively. Finally, the conclusions will be summarized in chapter six as well as suggestions for future work.

Chapter 2. Fundamentals of Laser Micro-fabrication

2.1 Techniques for Micromachining

There are many micromachining techniques such as chemical etching, electron/ion beam etching, X-ray lithography, extreme ultraviolet lithography, and laser fabrication. Clearly, the major driving force for the development of micromachining techniques is the rapid growth and fast progress in the semiconductor industry. Semiconductor industries, such as those based on Si and GaAs ICs, and optoelectronics, benefit from the rapid progress in micromachining.

The basic idea of practical chemical etching approaches is the same: to create a pattern in an etch-resistant material called footrests as seen in Figure 2.1 (a) and (b). In the subsequent etch process, the resist pattern is transferred to the underlying material where resist was absent, as shown in Figure 2.1 (c) and (d). The underlying material is removed. Material in the other region where it is protected by photoresist remains. The latent image is created in the resist by local exposure to ionizing radiation. Radiation induced chemical changes make the resist either more or less soluble when it is exposed to solvent developers. In chemical etching, the main disadvantage is the multi-step processing, which makes the semiconductor devices expensive. In addition, the sidewall effect is another problem [1].

2.1.1 Chemical Etching

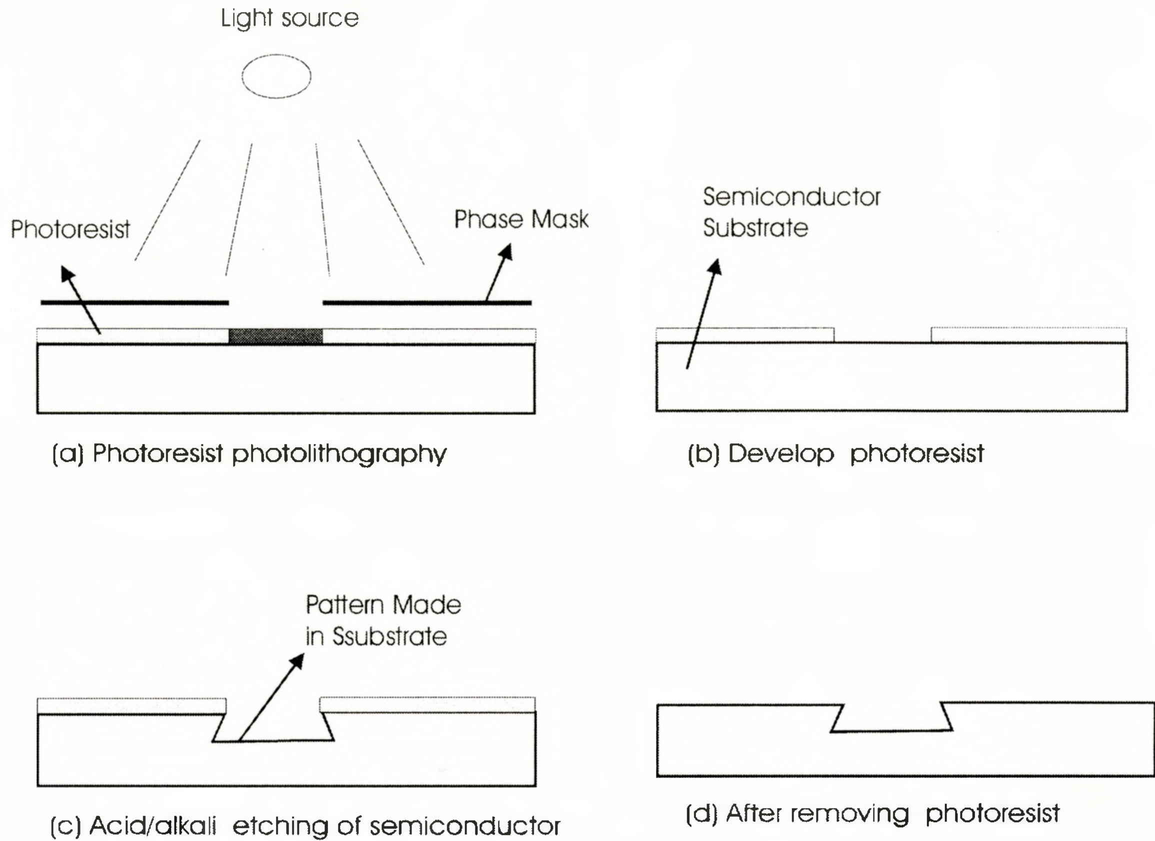

Figure 2.1: Traditional semiconductor chemical processing

2.1.2 Electron/Ion Beam Etching

In electron/ion beam etching, electrons/ions are accelerated to high energy and focused tightly onto the target. Because of the comparatively large particle mass, the electron/ion beam can be focused to about 5 nm (electron beam) and 1 nm (ion beam). The Figure 2.2 is the schematic view of electron beam projection system.

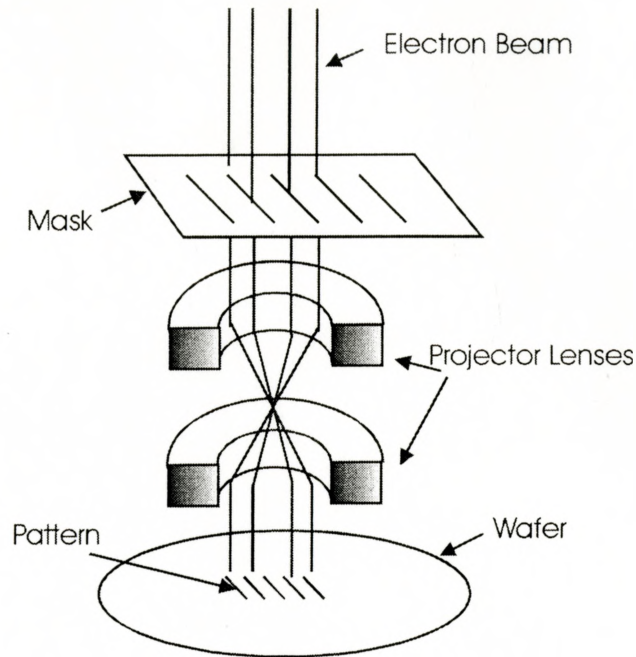

Figure 2.2: Schematic view of electron beam projection system

2.1.3 X-ray Lithography

For x-rays, the wavelength is normally 1 nm, and for the extreme ultraviolet lithography, in the region of 10 nm to 100 nm. X-ray approaches are based on the same basic idea of getting a good resolution in micromachining as with an electron/ion beam. The minimum resolved feature size R_{min} is mainly determined by the wavelength of the exposure light.

$$R_{min}=k_1(\lambda/NA) \qquad (2.1)$$

So with a short wavelength light beam, people can make features as small as ~100 nm [2]. The NA is the numerical aperture of the system, and k_1 is a factor ≥1 that describes how close the laser beam is to a perfect Gaussian beam.

At present, the x-ray and the extreme ultraviolet light source normally are spontaneous sources that are generated from plasma. Also the intensity of the x-ray or EUV light source is not high enough for direct machining. Normally, they are used to

develop masked photo-resist, and it actually is a step in traditional chemical etching micro-fabrication.

Another important area in micromachining is laser processing. Especially when ultrashort pulse lasers are used in lithography, thermal effects can be ignored so as to get features that are close to the size of laser wavelength because the heat has no time to spread out.

2.2 Introduction to Laser Micromachining

The current interest in the use of lasers is directly linked to the unique properties of laser light. The high spatial coherence achieved with lasers permits extreme focusing and directional irradiation at high energy densities. The monochromatic property of laser light, together with its tunability, opens up the possibility of highly selective narrow-band excitation [2]. Controlled pulsed excitation offers high temporal resolution and often makes it possible to overcome competing dissipative mechanisms within the particular system under investigation. The combination of all of these properties offers a wide and versatile range of quite different applications.

Materials processing with lasers takes advantage of virtually all of the characteristics of laser light. The high energy density and directionality achieved with lasers permit strongly localized heat- or photo-treatment of materials with a spatial resolution of better that 100 nm [3]. Pulsed lasers or scanned cw lasers allow time-controlled processing between about 10×10^{-15} s and continuous operation. The monochromaticity of laser light allows control of the depth of heat treatment or selective, non-thermal excitation either within the surface of the material and/or within the molecules of the surrounding medium - simply by changing the laser wavelength [2].

Because laser light is a massless tool, there is no need for mechanical holders with all the attendant problems these pose in the case of either brittle or soft materials. Furthermore, laser beams can be moved at speeds that can never be obtained by using mechanical tools or conventional heat sources. Contrary to mechanical tools, laser light is not subject to wear and tear. If this is properly controlled, it also guarantees constant processing characteristics. With medical and biological applications it is also important that laser beams are absolutely sterile tools [4]. Laser technology is completely compatible with present-day electronic control techniques. Naturally, a particular processing application will require only one or a few of these properties.

2.3 Materials Processing with Lasers

This discussion will be limited to a few types of lasers used in micromachining and materials processing applications. These lasers are neodymium-doped yttrium aluminum garnet (Nd:YAG) laser, CO_2 laser, excimer laser, and ultrashort pulse laser. The general advantages and disadvantages of lasers in materials processing are discussed.

The Nd:YAG laser is a solid-state laser which emits radiation at a wavelength of 1.06 μm. Power levels are available from a few Watts to over 1000 W average power. Applications are typically hole piercing, cutting, welding, and marking [5]. Nearly all these applications are for metals. Absorption coefficients for metals at this wavelength are fairly high. The typical Q-switched Nd:YAG lasers have about 200 ns pulse lengths with a pulse repetition rate of 10 kHz, and normal average power is in the region of a few Watts to a few tens of Watts. However, a serious drawback to Nd:YAG lasers has been the poor beam quality produced at high power levels. The cause was optical distortion of the beam in the YAG rod due to thermal lensing and other thermally induced

inhomogenities. This tends to produce a beam with poor mode quality, and consequently high divergence. High divergence translates to low brightness, bigger spot size and lower power density in the focused spot. It means lower resolution in micromachining. Anyhow, recent developments in Nd:YAG lasers have overcome this problem of large divergence to a significant extent. It is possible to drill a 1-inch thick steel plate in a few seconds with this solid state laser [6]. But this laser still cannot be used in micron resolution micromachining work because of the thermal effect that comes from the long pulse (over 100 ns). Besides, the long nanosecond laser pulse suffers from serious absorption in the laser induced plasma plume [3]. Considering the long pulse (ns-cw) laser ablation of materials (in Figure 2.3), there are always large heat affected zones and plasma plume shielding of the laser beams.

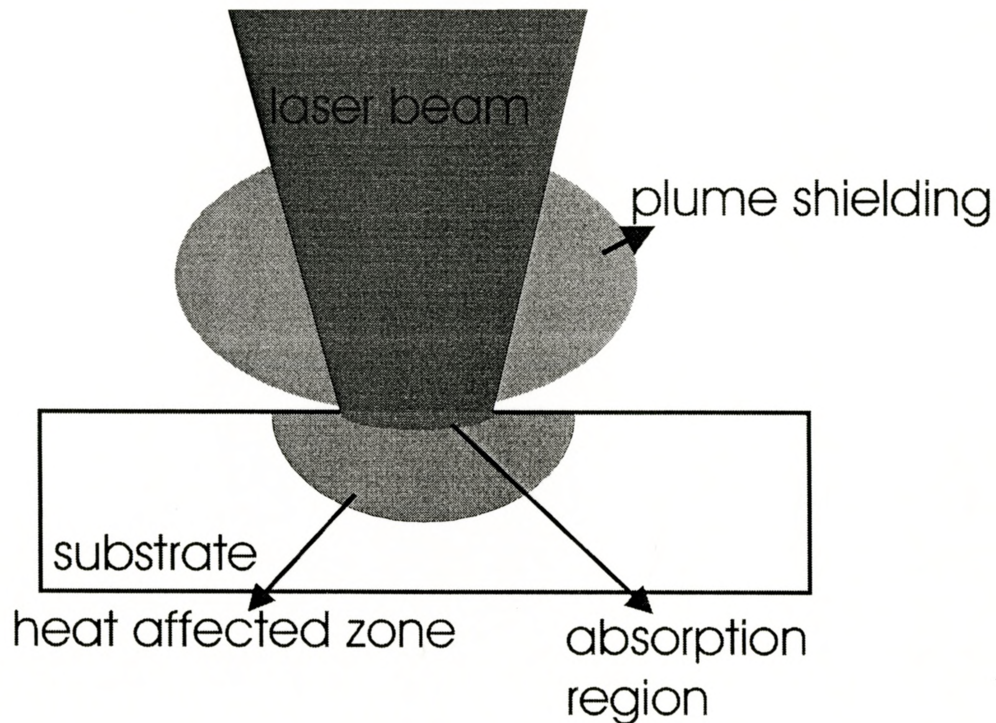

Figure 2.3: Diagram of long pulse laser ablation of material (Figure adapted from "Tutorial on laser micromachining", Potomac Laser Micro Tools, Inc)

The CO_2 laser has long been considered the workhorse of the material processing industry because of the wide power range available and the large variety of materials that can be processed with it. CO_2 lasers are working at a wavelength of 10.6 μm. All commercial CO_2 lasers can be classified in one of several basic designs. The low power lasers, operating at less than 100 W, utilize a sealed off design. The conventional types are waveguide designs and glass tube design. In the waveguide type CO_2 lasers, the core of the tube is so narrow that it acts as a waveguide. The output of these low power lasers is very near Gaussian. The gas fill in these lasers must be replaced periodically. Medium to high power CO_2 lasers are normally fast transverse flow with transverse discharge. Average power ranges from 100 W to 25 kW [5]. It is common to use an unstable resonator in CO_2 lasers to operate at over a kW. The purpose is to get a bigger gain volume and decrease the power density in the cavity so as to get a high power oscillation and also protect the cavity mirrors. High power CO_2 lasers are very big since the laser medium is gas. Normally, continuous wave operation is applied to this laser. So high power CO_2 lasers are often used in thick metal sheet cutting, metal welding and annealing. It is not a good idea to use this large-scale laser in micromachining semiconductors or dielectrics.

Another important laser that is widely used in industry is the excimer laser. The term excimer is literally a contraction of the phrase - excited dimer [2]. A dimer is a molecule containing two identical atoms. The molecules in most widely used excimer lasers are actually complexes because they are composed of a halogen and a noble gas atom. There are several gas combinations that lead to excimer laser operation. All emit radiation in the ultraviolet region of the electromagnetic spectrum. The combinations and

the wavelengths at which they emit are ArF, 193 nm; KrF, 248 nm; XeCl, 308 nm; and XeF, 351 nm. The laser pulse duration ranges from ns to ps. There are numerous applications for excimer lasers in micromachining of thin metal sheets, wide band gap materials and polymers, marking, and microelectronics. Because of their short wavelength and fairly short pulse length, they interact differently with materials than a traditional materials processing laser. When an excimer laser is used to drill or cut wide band gap materials such as polymer or glass, there is virtually no prominent evidence of thermal interaction. The short wavelength allows direct interaction with chemical bonds, instead of building up enough heat to break them, which takes times and allows thermal conduction away from the direct interaction zone. However, since the normal excimer laser has a duration of ns, it is still comparatively long when considering the heat conduction in materials such as metals. From the thermal effect, the ultrashort pulse lasers, which are working in the pulse duration region of ps to fs, are better than excimer lasers.

2.4 Ultrafast Laser Micromachining

Ultrashort pulse duration is extremely short, and the electric field is high enough to ionize any material via single or multi-photon absorption. Ultrashort pulse lasers will be strong candidates for microstructural fabrication in addition to UV lasers.

The ultrashort pulse duration in some respects fundamentally changes the laser-matter interaction mechanisms. The short duration also means that the hydrodynamic motion of the matter under laser irradiation can be ignored as shown in Figure 2.4 (a), and there is essentially no fluid dynamics to consider during the laser-matter interaction. The energy deposition takes place at the solid density, as opposed to the long-pulse case

where the absorption mainly happens at the critical plasma density layer. On the other hand, the interaction is highly non-equilibrium, with electrons driven to much higher temperatures than the ions. Subsequent electron-ion energy relaxation takes place on a much longer time scale than the laser-matter interaction time [7].

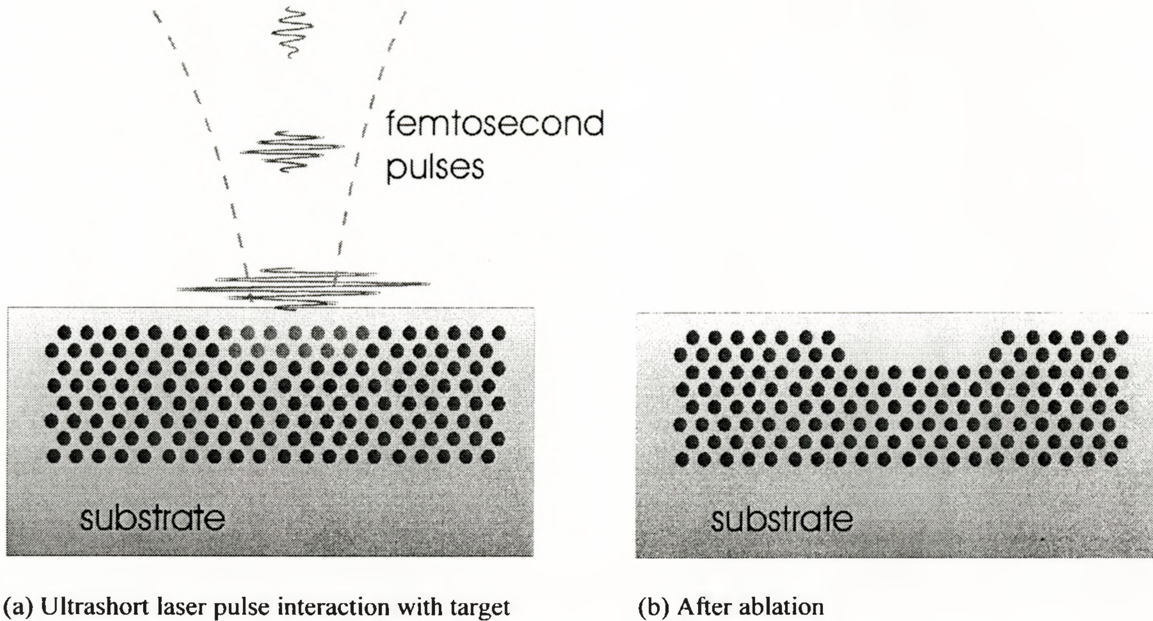

(a) Ultrashort laser pulse interaction with target (b) After ablation

Figure 2.4: Ultrafast laser ablation of material (Figure adapted from "Micromachining handbook", Clark-MXR, Inc)

Picosecond- and femtosecond-laser ablation has been proved to be a powerful technique for the patterning of both thermally high-conductance materials such as metals, and wide-bandgap materials, such as dielectrics. Because both the influence of heat conductivity within the material and screening of the incident laser light are strongly diminished with picosecond pulses, and can even be largely ignored with femtosecond pulses, material removal is very localized as shown in Figure 2.4 (b) and requires less energy.

With ultrashort pulses, ablation mechanisms that are of minor relevance or not at all present in nanosecond-laser ablation, become increasingly important. These include non-linear optical absorption, non-equilibrium effects related to electronic and/or vibration excitations, avalanche breakdown, multi-photon ionization (MPI), and phenomena related to overcritical heating [4]. Such strongly non-linear interaction processes can further enhance the localization of the excitation energy. This increases the resolution (sub-wavelength) in surface patterning and also opens up novel material-processing possibilities.

For laser ablation of wide band gap materials such as dielectrics, multi-photon ionization (MPI) (see Figure 2.5) must be considered. In these cases, a single photon cannot excite an electron from the valance band to the conduction band in a wide band gap material. However, an electron can make a transition from the ground state to the excited state by the simultaneous absorption of two or more laser photons. The absorption of photons from the laser beam increases nonlinearly with laser intensity according to the relation

$$R = \sigma^{(n)} (I/h\upsilon)^{n} \tag{2.1}$$

where $\sigma^{(n)}$ is a coefficient that describes n-photons absorption. The approximate cross section $\sigma^{(n)}$ is: $\sigma^{(2)} \sim 10^{-34}\text{-}10^{-50}$, $\sigma^{(3)} \sim 10^{-51}\text{-}10^{-80}$, $\sigma^{(4)} \sim 10^{-68}\text{-}10^{-140}$ ($\mathrm{cm}^{2n}\ \mathrm{s}^{(n-1)}$) [3]. The intensity I is in the region of $10^{12}\text{-}10^{14}\ W/cm^{2}$ in the case of femtoseond laser micromachining.

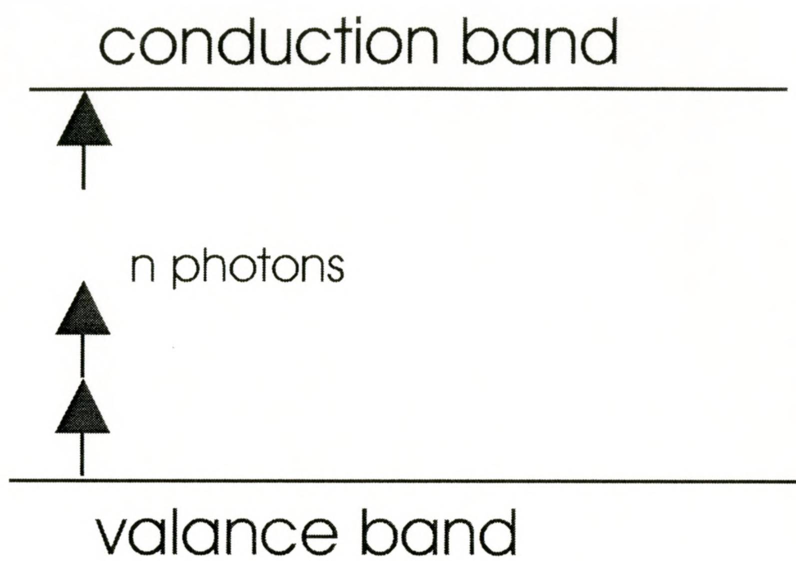

Figure 2.5: Diagram of multi-photon absorption

Chapter 3. Ultrashort Pulse Lasers

3.1 Introduction

Ultrashort pulse lasers rely on the process of mode locking to generate short optical pulses. The term mode locking originates from the description of the pulse formation process in the frequency domain. A typical free running laser cavity can operate on as many as 100,000 longitudinal modes [8]. The exact number of modes depends on the bandwidth of the gain medium and the cavity geometry. If there is no fixed phase relationship between the cavity modes, the laser output will be continuous wave (cw) emission under the case of no Q-switching. However if the cavity modes are phase locked they will add coherently and interfere constructively. The output of a mode-locked laser is then a train of short, intense pulses separated temporally by the cavity round trip time [7].

The typical ultrashort pulse lasers are dye lasers, Ti:sapphire laser, and various Cr-doped lasers such as Cr:LiSAF laser. They are commercially available from companies such as Spectra Physics, Clark-MXR etc. Dye lasers that are normally mode-locked by a saturable absorber were widely used before the solid state ultrashort pulse lasers became widespread. However, since solid state lasers have better optical and physical properties and are more easily operated and maintained, they are often used now instead of dye lasers. Also, for the Ti:sapphire laser, it has a larger gain bandwidth than dye lasers.

Numerous methods have been developed to generate ultrashort laser pulses. In general, these methods can be classified into three basic categories: mode locking, gain switching, and shaping and compression of existing pulses. Kerr-lens mode locking (KLM) has revolutionized femtosecond pulse generation in solid-state materials because the KLM technique produces the shortest pulses, and it is relatively simple to implement [2]. As shown in Figure 3.1, when a intense laser pulse passes through a Kerr medium, the laser pulse suffers from the Kerr effect which comes from the third order nonlinear effect and leads to self-focusing in the Kerr medium. So, by engineering design of the laser cavity, people can use this nonlinear effect to realize the mode locking by which only the self-focusing ultrashort laser pulses can oscillate inside the laser cavity. If the peak power of the pulses obtained from a Kerr-lens mode-locked oscillator is insufficient for a particular application, the pulse can be amplified by means of chirped pulsed amplifier (CPA), which will be discussed later. The Ti:sapphire crystal has an extremely wide fluorescence bandwidth, which could theoretically support 3 fs pulses; the shortest pulses that have ever been achieved are around 4.5 fs in the Ti: sapphire laser [4].

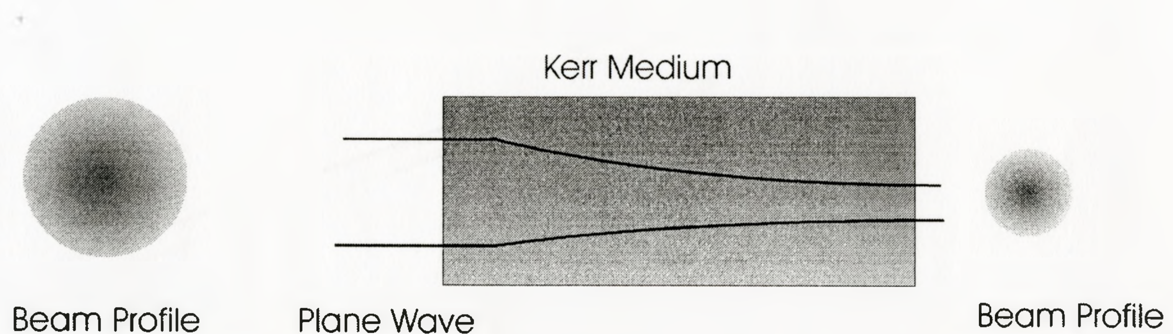

Figure 3.1: Kerr lens mode locking

3.2 Group Velocity Dispersion and Dispersion Compensation

Fourier analysis imposes a restriction on the bandwidth of an ultrashort pulse. For a pulse of duration Δt_p and bandwidth $\Delta \nu$, it is always true that [9]:

$$\Delta \nu \bullet \Delta t_p = \alpha, \ \alpha \geq 1, \tag{3.1}$$

The size of α depends on how much the pulse is dispersed. It is apparent that the shorter the pulse, the larger the bandwidth, and thus the greater the difference from the lowest to highest frequency component. Each frequency in a pulse experiences a slightly different index of refraction as it propagates. This index of refraction difference corresponds to a velocity difference, causing a time separation between the different frequencies of a pulse. Group velocity dispersion (GVD) [10, 11] is defined as the variation in transit time as a function of wavelength. The second derivative of the refractive index with respect to wavelength, $d^2n/d\lambda^2$, determines the GVD. It also governs the rate at which the frequency components of a pulse change their relative time. GVD can change the temporal shape of the pulse by broadening it or narrowing it, depending on the chirp of the original pulse. A pulse is said to be positively chirped when it has experienced positive GVD, if the low frequencies lead the high frequencies, and negatively chirped if the opposite case is true [10]. Pulses are typically positively chirped as they pass through normal materials at visible and near IR wavelengths. The effect is more significant for shorter pulses because of their extremely large bandwidth.

In addition to GVD, the output pulse width and pulse shape from the ultrashort pulse laser suffer from the nonlinear effect-self phase modulation (SPM) [11]. The self phase modulation can be described in terms of the intensity-dependence of the refractive index:

$$n = n_0 + n_2 I \tag{3.2}$$

where n_0 is the linear refraction index and I is the pulse intensity. As the pulse propagates through a nonlinear material such as the gain medium (Ti:sapphire) in an ultrashort pulse laser, the leading edge experiences an increasing index of refraction. This causes a delay in the individual oscillations of the electric field and results in a "red-shifted" leading edge. On the contrary, the trailing edge of the pulse is "blue-shifted". So, SPM will broaden the spectrum of the pulse and provide a positive chirp.

In order to achieve ultrashort (in femtosecond region) output pulses, it is necessary to compensate for the pulse spreading caused by positive GVD and SPM. There are many ways to realize dispersion compensation, such as prism pairs, grating pairs, etc. In our Tsunami oscillator, the positive dispersion is compensated by prism pairs (see Figure 3.2).

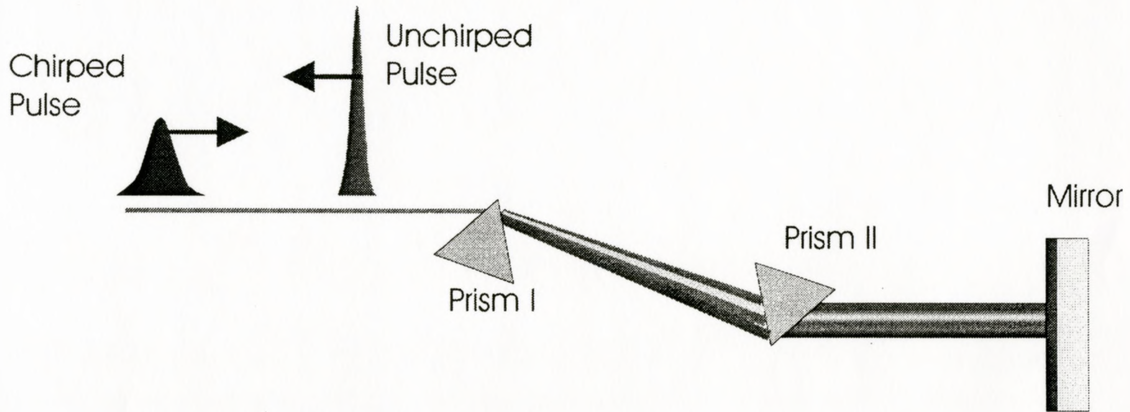

Figure 3.2: Dispersion compensation with prism pair

As discussed earlier, a material exhibits GVD when the second derivative of its refraction index, with respect to wavelength ($d^2n/d\lambda^2$), is non-zero. This is a special case that is only valid when all wavelengths follow the same path through a material. This can be extended to any optical system having a wavelength dependent path length (P). GVD

is then governed by the second derivative of the optical path with respect to wavelength ($d^2P/d\lambda^2$) [10]. Therefore, a prism pair in Figure 3.2 can be used to produce negative GVD. This is generally the preferred intra-cavity compensation technique for ultrashort pulse lasers because losses can be minimized by using the prisms at Brewster's angle, and the negative GVD is nearly linear over a larger bandwidth [9].

3.3 Chirped Pulse Amplification in Ultrashort Pulse Lasers

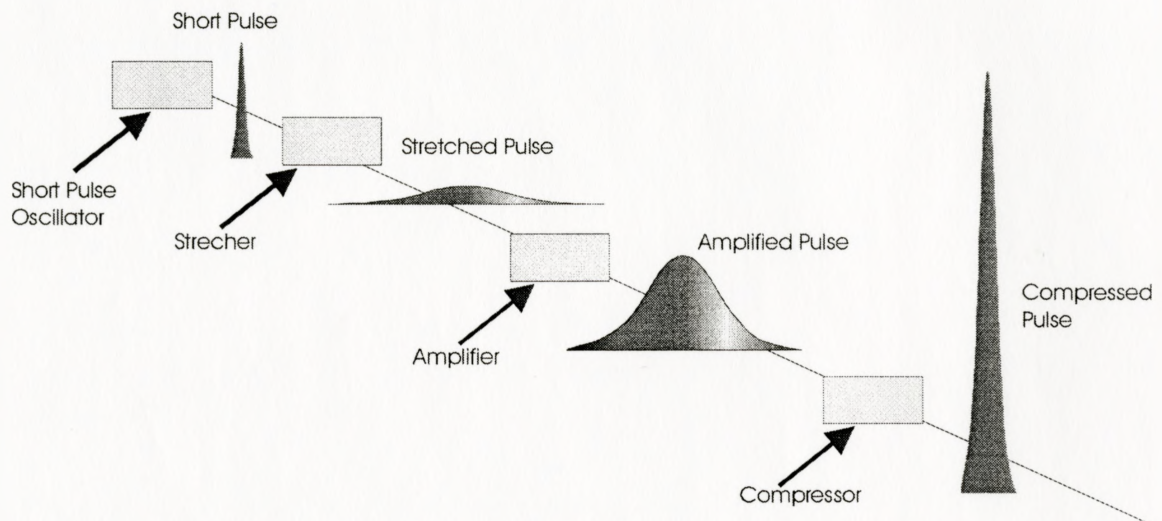

Figure 3.3: Diagram of CPA (Figure adapted from the CLEO 2001 short course "Fundamental of ultrashort pulse amplification", C. P. J. Barty, Lawrence Livermore National Lab)

Usually the ultrashort pulse laser oscillator operates at a pulse repetition rate of about 100 MHz, and the pulse energy is in the range of nano-Joules. Amplification to the micro-Joule and mille-Joule level is needed for many applications, including micromachining. However, the pulses cannot be amplified directly because the high intensity level of the short pulses inside the amplifier will damage the optical components. The effect of self-focusing associated with high-intensity pulses makes the situation even worse [7]. To overcome this limitation, the technique of Chirped Pulse Amplification (CPA) [7, 9] has

been developed and is now widely used in ultrashort pulse laser technology. Briefly, the idea of CPA is shown in Figure 3.3. A very short duration pulse is initially generated in oscillator. The next step is to stretch its pulse duration in the stretcher, thus significantly reducing its brightness (or peak power). This low brightness optical pulse is then amplified, with a low probability of self-focusing inducing damage. After amplification, the pulse is recompressed via a compressor to near its original duration.

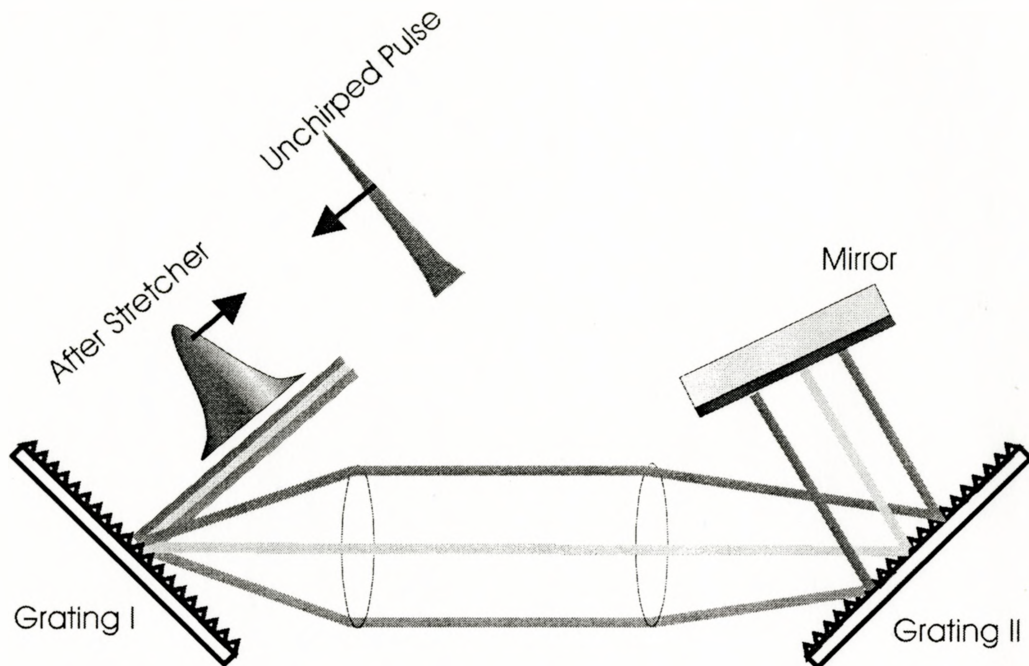

Figure 3.4 (a): Stretcher

Pulse stretching and compression can be achieved with the use of diffraction gratings. In a pulse stretcher (see Figure 3.4 a), the input beam is incident on a diffraction grating, causing the different frequencies present to disperse. The grating can be configured in such a way so that the blue frequency components have to travel further through the stretcher than the red components. The result is that the red components exit the stretcher first and the pulse has been stretched.

The pulse compression is the reverse of pulse stretching. The gratings are arranged so that the blue frequency components travel the shorter path and therefore catch up with the red frequency components. In the end, the pulse is compressed.

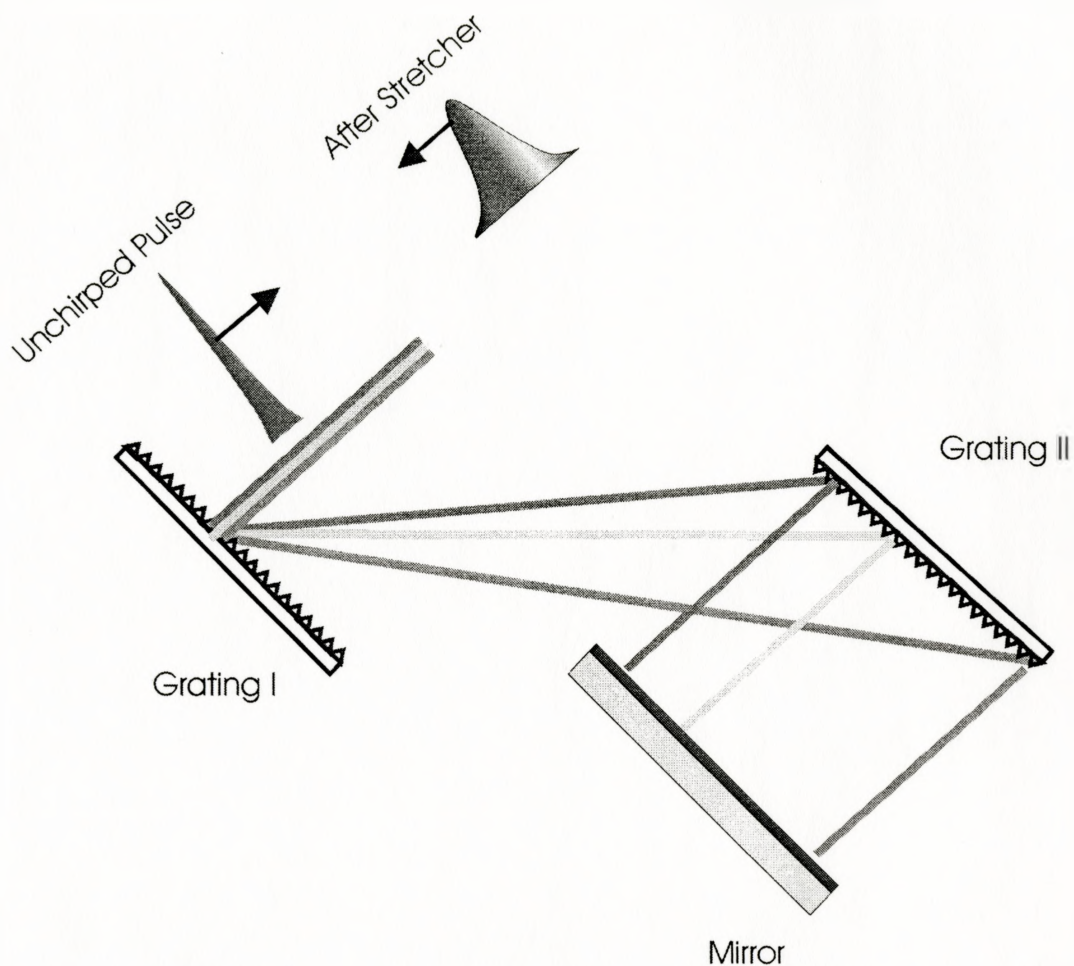

Figure 3.5 (b): Compressor

3.4 Time Domain Measurement of Femtosecond Laser Pulses

The advent of femtosecond lasers brought a new problem of measurement. The direct combination of a photodiode and an oscilloscope is no longer adequate to temporally resolve the ultrashort pulses generated [30]. The fastest optical detectors have response

times ~10^{-11} seconds and so they are unable to measure pulse durations shorter than a few tens of picoseconds. The only thing fast enough to measure these pulses is the pulse itself. The most common form of autocorrelation is by second harmonic generation.

The technique of autocorrelation allows the conversion of the difficult problem of measuring time scales in the order of 100's of femtoseconds into the much easier task of measuring lengths of the order of microns. For instance 100 fs has an equivalent optical path length of 30 μm in air.

Most autocorrelators are based on the Michelson interferometer design (see Figure 3.5) [12], where the pulse under investigation is split into two pulses by a beamsplitter and each pulse is sent through a separate arm. Changing the length of one arm introduces a time delay τ for the pulse in that arm. The two pulses are recombined by the same beamsplitter and frequency doubled in a nonlinear crystal. The second harmonic signal intensity will reach a maximum when two pulses arrive in the crystal at the same time ($\tau=0$) and the signal will drop to zero when the two pulses do not overlap temporally. The intensity autocorrelation is given by:

$$A^{(2)}(\tau) \equiv \int_{-\infty}^{\infty} I(t) \bullet I(t-\tau) \bullet dt \tag{3.3}$$

Therefore the second harmonic signal roughly corresponds to the pulse width.

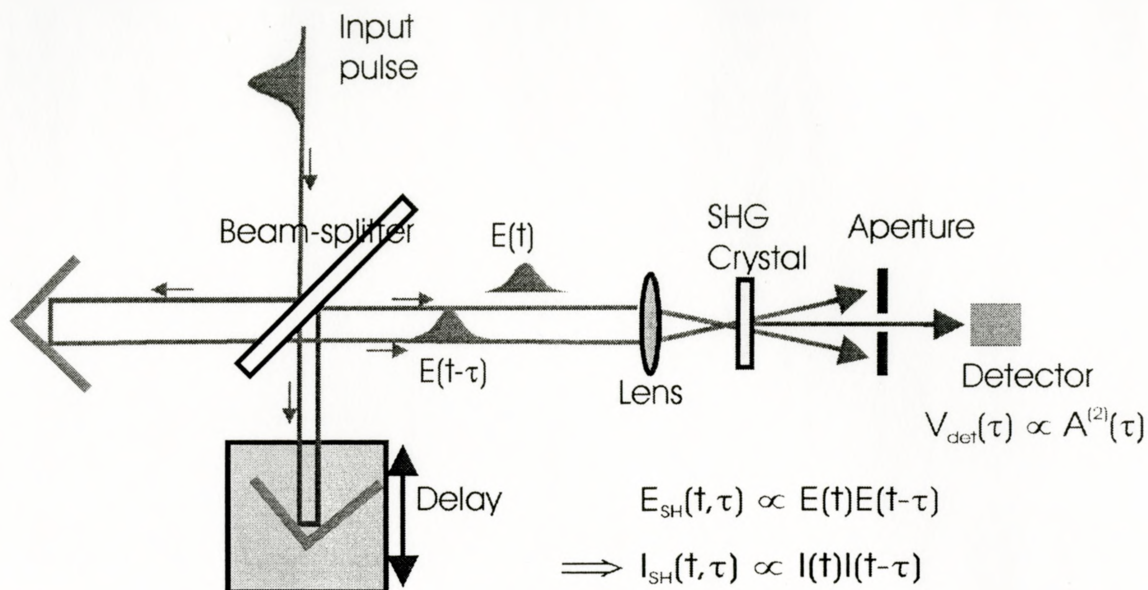

(a) Diagram of autocorrelation

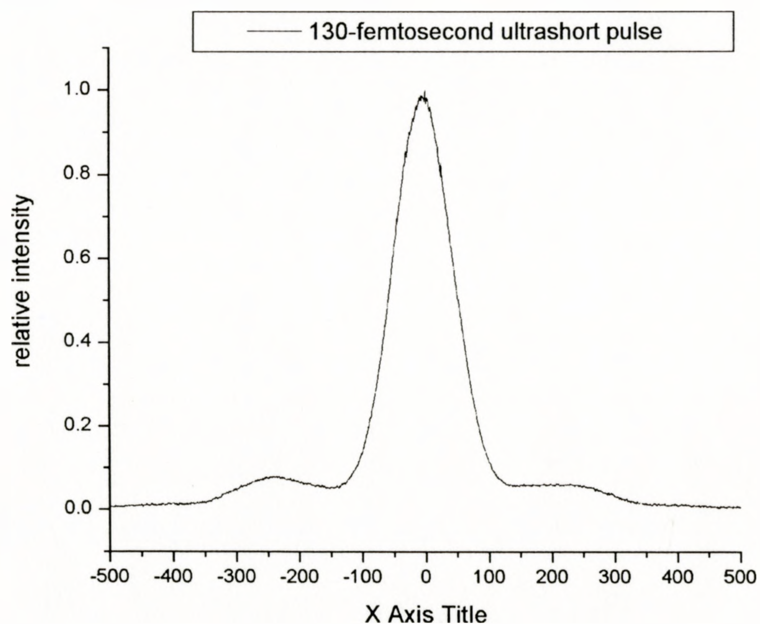

(b) 130 fs laser pulse measurement result

Figure 3.6: Diagram of autocorrelation and measurement result of a 130 fs pulse

Chapter 4. Femtosecond Laser Ablation of Dielectrics

4.1 Introduction

As discussed in chapter 2, there are a number of advantages in using lasers for micromachining: single-step processing, high flexibility, direct writing of structures by moving the laser beam, no contamination of the material, leading to highly localized treatment of materials with spatial resolution of better than 1 μm. However, this high spatial resolution normally cannot be achieved by using standard nanosecond lasers due to strong thermal effects that occur in the material and the destructive influence of the plasma that is formed above the surface. Dielectric materials require very high laser intensity with normal ns lasers in order to obtain sufficient energy absorption in the material to remove material. The thermal stress that is built in the material during and after the long laser pulse leads to cracking and explosive destruction of the sample as shown in Figure 4.1 (left) which is made by 5 nanosecond laser pulses (λ=351 nm, τ=138 ns with near-threshold fluence ~314 J/cm^2) in fused quartz. The laser beam was focused into ~5 μm, but over ~50 μm cracked crater was made.

There are two ways to overcome these problems. One is reducing the wavelength of the laser pulses in order to increase the absorption cross-section. The second approach is to reduce the pulse duration of the laser [13]. As shown in Figure 4.1 (right) which is a crater made in fused quartz by irradiation with a sequence of five femtosecond laser pulses (λ=790 nm, τ=130 fs) focused into ~6.3 μm (1/e^2 of intensity) spot with a single

pulse fluence ~1.5 J/cm^2 which is close to ablation threshold, there are no visible cracks in ablation region. There are many advantages of using ultra-short laser pulses with pulse duration below 10 ps in laser ablation of dielectrics: much less energy input is required to produce the same amount of material removal; thermal damage around the irradiated area is much reduced; multi-photon excitation can achieve smaller structures; there is no laser interaction with the ablated particles, and no laser shielding.

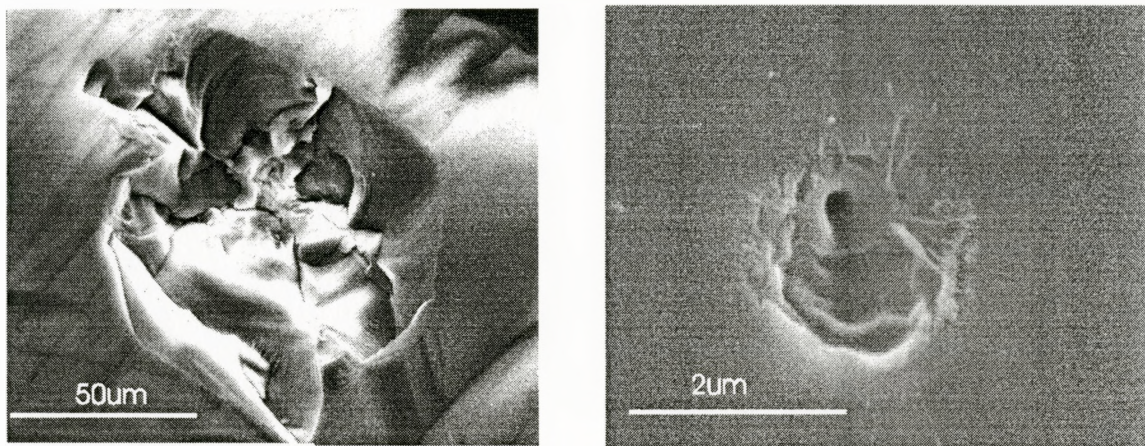

Figure 4.1: (left) Cracks in fused quartz induced by five nanosecond laser pulses (λ=351 nm, τ=138 ns with fluence ~314 J/cm^2), (right) crater in fused quartz made by five femtosecond laser pulses (λ=790 nm, τ=130 fs with fluence ~1.5 J/cm^2), no cracks

4.2 Motivations and Background

Research on the detail of features induced by ultrashort laser pulses is essential for the coming applications in the future. For example, we need to know how smooth the craters are, and how deep they are. How efficient is it to use femtosecond lasers in micromachining? How much energy do we need to do this job? In addition, we need to know how much debris is around the features after ablation. In order to answer some of

these questions, we selected fused silica and another often used material BK7 in our experiments. Both of these materials have high transmission from the UV to the IR and outstanding thermal, electrical and chemical properties. Conventional machining of these materials is rather difficult, if small or complex shaped components are required. Excimer lasers have been used for this purpose. However, because of the poor beam quality, the resolution is not really that good [2]. The solid state ultrashort pulse laser is another competitive candidate for this industry.

Although femtosecond lasers are still complex and expensive, the technological developments are presently occurring at such an extremely fast pace that small, friendly, relatively inexpensive, solid state systems with sufficient intensity for the applications should be available in the very near future.

In this chapter, we present the processes occurring when dielectric materials are irradiated with ultrashort laser pulses. We will focus on near infrared (~790 nm) micromachining. In addition, there are some preliminary ablation results on UV (~395 nm) and infrared ~1300 nm ultrashort laser pulse machining. Pulse durations are in the region of 100 fs to 1700 fs by using the method of changing the relative position of compressing gratings.

There have been a number of studies [13-26] of the ultrashort pulse laser pulses induced damage in transparent materials. The E.E.B. Campbell group [13-19] did a lot of detailed work on the ultrashort laser irradiation and ablation of dielectric materials, including sapphire [14, 15, 17], quartz [14, 16, 19], CaF_2 [19] etc. Their interests cover almost all the aspects of the ultrashort pulse laser micro-structuring of wide bandgap materials, including machining in the time regime from fs to ns [17] and spectrum regime

[18]. They investigated the morphology of several dielectrics irradiated by laser light at a wavelength of 790 nm for different pulse widths (between 200 fs and 5 ps) [17] and fluences near the single shot ablation threshold via complementary techniques of electron microscopy and atomic force microscopy. They observed differences that relate to the mechanisms and dynamics of defect production in wide band gap materials. They also talked about the single- and multi-shot damage threshold and ablation threshold for dielectrics as a function of laser pulse width (190 fs-4.5 ps) [19]. They thought that both the damage threshold and ablation threshold decreased with decreasing pulse width over the entire pulse-width range investigated. Also, they found that a clear improvement in the quality of the ablated structures for multiple-shot ablation as the pulse width is decreased [18]. By detecting the scattered light signal of a probe pulse [14], they determined the electron-phonon coupling strengths of different dielectrics. They found the amorphous quartz is a material with very strong electron-phonon coupling strength in contrast to sapphire and MgO which both are in the category of materials with intermediate electro-phonon coupling strength. They also used the time-of-flight mass spectrometer to investigate the mass and velocity distributions of positive ions produced by fs laser ablation of sapphire [15].

M. Lenzner et al [22, 24, 25, 26] also reported on femtosecond laser ablation of dielectrics. They presented experimental ablation results in glasses with single and multi-shot irradiation in the 10 fs pulse duration domain [26]. One interesting phenomenon that they found is that the lateral precision deviates from the theoretically predicted one in the >100 fs regime; in contrast, in the 10 fs regime the measured lateral extension parameter [26] shows good agreement with the prediction. Therefore, they believe that laser pulses

in the 10 fs regime offer a significantly improved lateral ablation precision in dielectrics as compared to standard sub-picosecond pulses. From these results, they demonstrated that these extremely short pulses offer the potential for lateral and vertical machining precision of the order of 100 nm.

Some other groups such as D. Du et al [20], Stuart et al [21], and A. Tien et al [23] also reported the relationship between the laser pulse duration and damage threshold in ultrashort pulse laser ablation of dielectric materials. Our work is similar to that of the Campbell group. We both did single shot and multi-shot irradiations analyzed with SEM and AFM. Also, we too realized UV (~395 nm) machining. However, beyond these similarities, we also investigated 1300 nm ultrashort laser pulse machining. Also we used the model in J. Bonse's publication [29] to carefully fit the squared crater diameter to the laser fluence so as to get ablation thresholds in materials instead of viewing the visual damage which is limited by optical or electron microscopes and human errors. In addition, we particularly investigated in detail the evolution of surface features in multi-shot patterns.

4.3 Experimental

A kHz-rate Ti:sapphire amplifier system delivering sub-130 fs pulses of energies up to 300 μJ at ~790 nm was used for the micromachining experiments. The amplified laser pulses were attenuated by a half-wave plate and a polarizer to pulse energies of 10 μJ and below. Before the micromachining setup (Figure 4.2) [30], the energy was adjusted with a set of neutral density filters in steps of 0.1 OD ($OD=\log(I_o/I)$). The laser was focused on the sample in a stainless steel vacuum chamber by a 10× microscope objective (NA: 0.25) or a gradient index lens (f: 30mm) giving a $1/e^2$ (intensity) irradiated area of ~31

μm^2 and ~64 μm^2 (at λ =790 nm) respectively. The vacuum chamber and the sapphire window provide a strong attenuation of soft x-ray radiation that comes from the laser machining. When higher pulse energies were used (>2 μJ/pulse), additional shielding (a lead-doped plastic) was also employed, and localized movable shielding blocks were at times incorporated close to the microscope objective. A scanning knife-edge measured the spot sizes. The beam shapes (λ =790 nm and λ =395 nm) obtained with focusing by the 10× objective are shown in Figure 4.3.

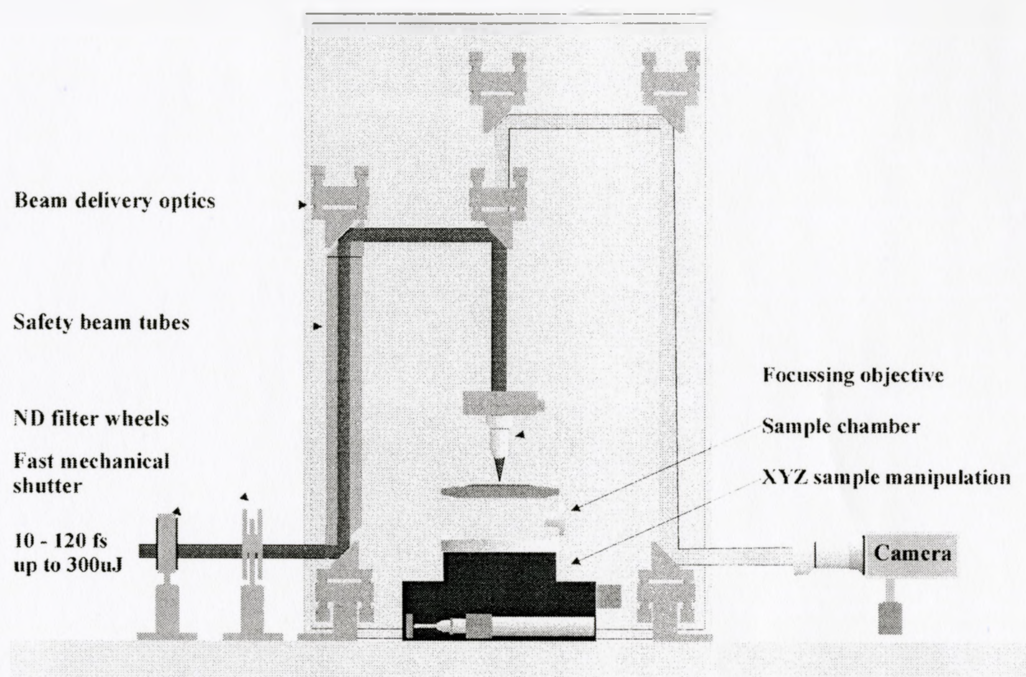

Figure 4.2: Micromachining setup (Figure provided by A. Borowiec)

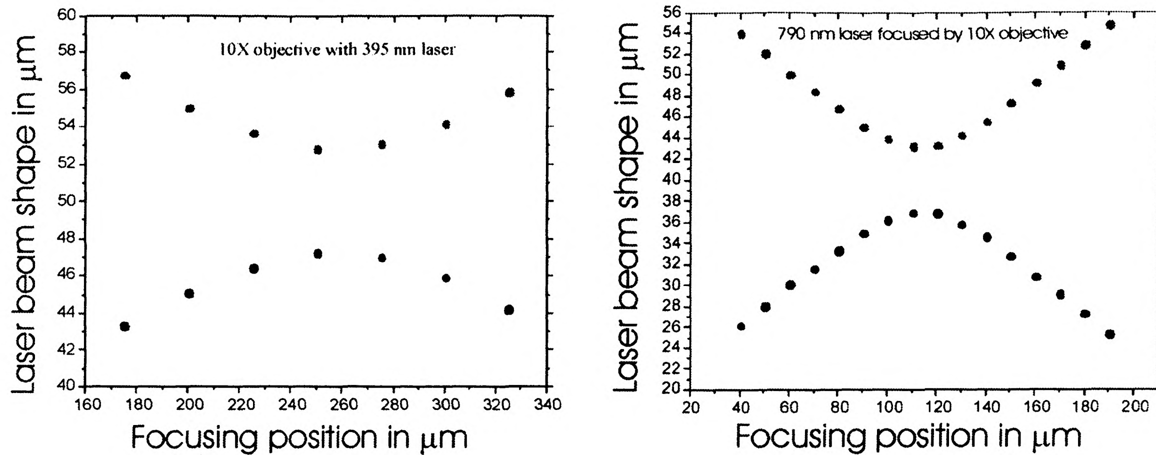

Figure 4.3: (left) 395 nm (from doubling frequency of 790 nm laser) laser beam shape focused by a 10× objective; (right) 790 nm laser beam shape focused by a 10× objective

A fast mechanical shutter, synchronized with the laser, was used to control the number of pulses delivered to the sample. A confocal imaging system and a CCD camera were used to monitor the machining process. A vacuum chamber was mounted on a computer controlled xyz translation stage with minimum step size of 0.5 µm. The laser beam was delivered through a thin (200 µm thick) uncoated sapphire window cut perpendicular to the c-axis to avoid birefringence effects in the window.

4.4 Single-Shot Results and Discussion

In our dielectric ablation experiments two ablation phases can be identified. The first is a gentle ablation characterized by a low rate of material removal that was attributed to particle vaporization. The second phase characterized by a high rate of material removal and the production of molten droplets or even cracks which was attributed to phase explosion. Further details about the two phases ablation is beyond the scope of this thesis; interested readers are referred to [13, 15]. Anyhow, we often confine the laser energy in 5 µJ/pulse, fluence 16 J/cm^2, which is in the first ablation region.

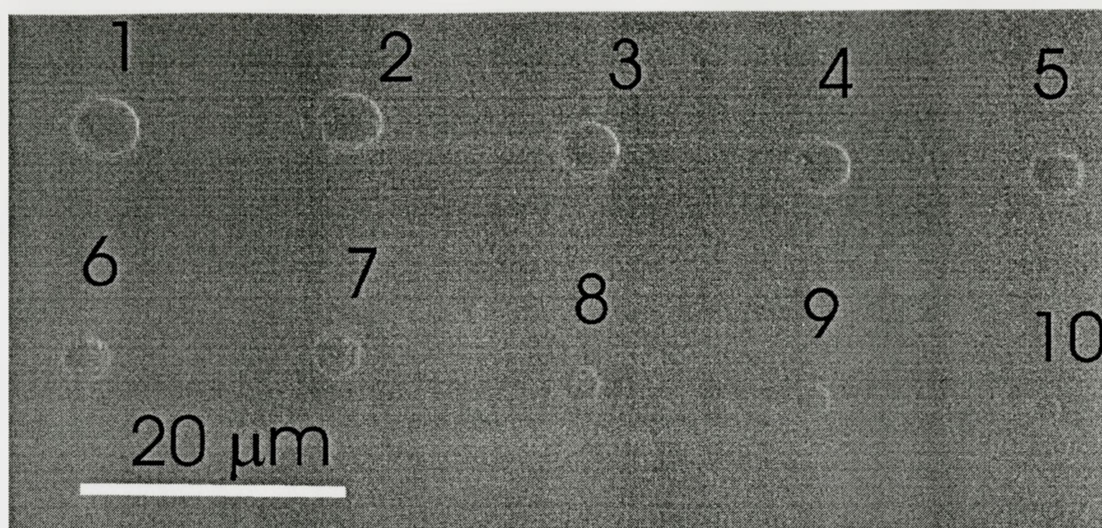

Figure 4.4 (a): SEM image of the fused silica single-shot ablated at different fluence (from 5.1 J/cm² to 0.64 J/cm²) by single laser pulse (τ=130 fs, λ=790 nm)

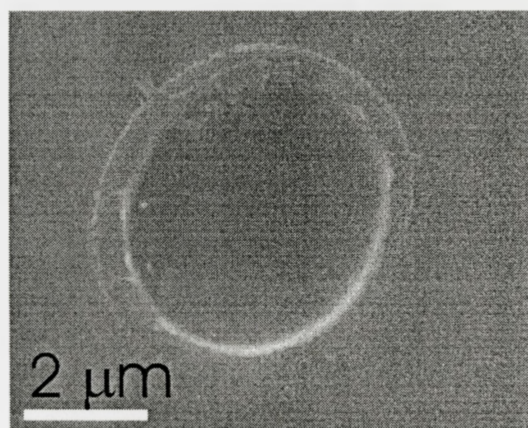

(b)

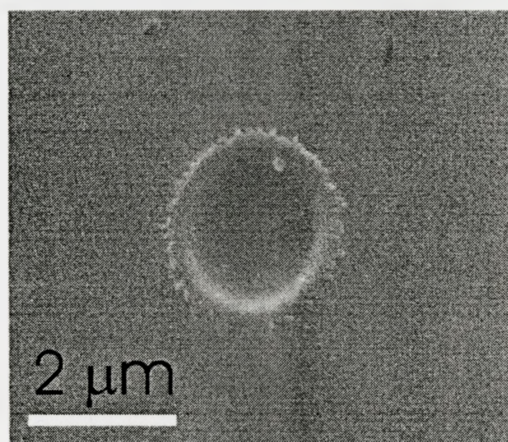

(c)

Figure 4.4 (b): Zoom view of the crater #1 which is made with a laser fluence of 5.1 J/cm²

Figure 4.4 (c): Zoom view of the crater #10 which is made with a laser fluence of 0.64 J/cm²

Figure 4.4 (a) is a SEM photograph of craters made by single laser pulse (λ=790 nm, τ=130 fs) with laser fluence from 5.1 J/cm^2 to 0.64 J/cm^2. As we have seen from Figure 4.4 (a), the lateral dimensions of the craters are dependent on the fluence of the laser pulse. The higher the fluence the bigger the crater is. There is a physical relation

between the lateral dimension D and the single laser pulse fluence ϕ_0 From the model of J. Bonse [29], for a Gaussian beam, the spatial fluence profile is given by [28]

$$\phi(r) = \phi_o e^{-2r^2/w_0^2} \quad (4.5.1)$$

where r represents the distance from the beam center, w_o is the 1/e^2 radius of the intensity distribution; ϕ_0 denotes the maximum fluence, and the pulse energy E_{pulse} and ϕ_0 are directly related by

$$\phi_o = 2E_{pulse}/\pi w_o^2 \quad (4.5.2)$$

With an ablation threshold fluence ϕ_{th}, the diameter D of an ablated crater is also related to the maximum fluence:

$$D^2 = 2w_o^2 \ln(\phi_o/\phi_{th}) \quad (4.5.3)$$

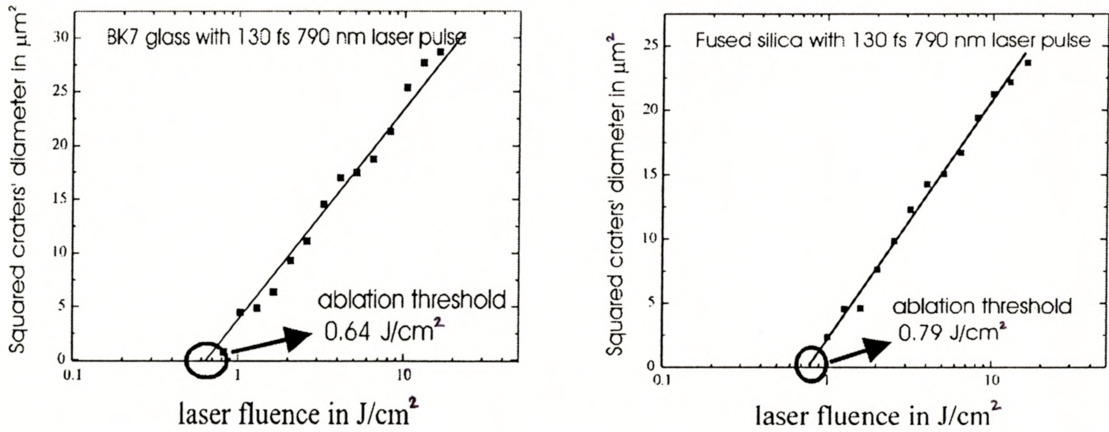

Figure 4.5: Squared diameter D^2 of the ablated craters in BK7 (left) and fused silica (right) as a function of the laser fluence ϕ_o (λ=780 nm, τ=130 fs)

Due to the linear dependence of the maximum laser fluence on the total pulse energy, it is possible to determine both the beam radius and hence the threshold fluence from the plot of the square of the crater diameter versus the logarithm of the pulse energy. The slope is the linear fit in Figure 4.5 to the data. Above all, the slope is quite

linear. The zero value of D^2 yields the ablation threshold fluence ϕ_{th} which is ~0.64 J/cm^2 in BK7 glass and ~0.79 J/cm^2 in fused silica from the Figure 4.5. Compared to the literature, our result of ablation threshold on fused silica is relatively low. A. Tien et al. [23] reported that the ablation threshold of fused silica at 800 nm laser pulse (τ=100 fs) is ~3.5 J/cm^2; while the result from M. Lenzner et al. [22] is ~2 J/cm^2 with the 220 fs laser pulse (λ=780 nm). We think that the difference comes from our laser pulse energy measurement and spot size measurement; besides the fused silica samples are another possibility. Our fused silica sample is Dynasil 4000 or equivalent fused silica glass from Coherent. But we cannot get any information about the fused silica samples that Lenzner group and Tien group used. There are types of fused silica glass which have different compositions, so the ablation threshold could easily be different to some extent. In addition, possible "prepulse" issues could also play a role in the differences observed between various groups.

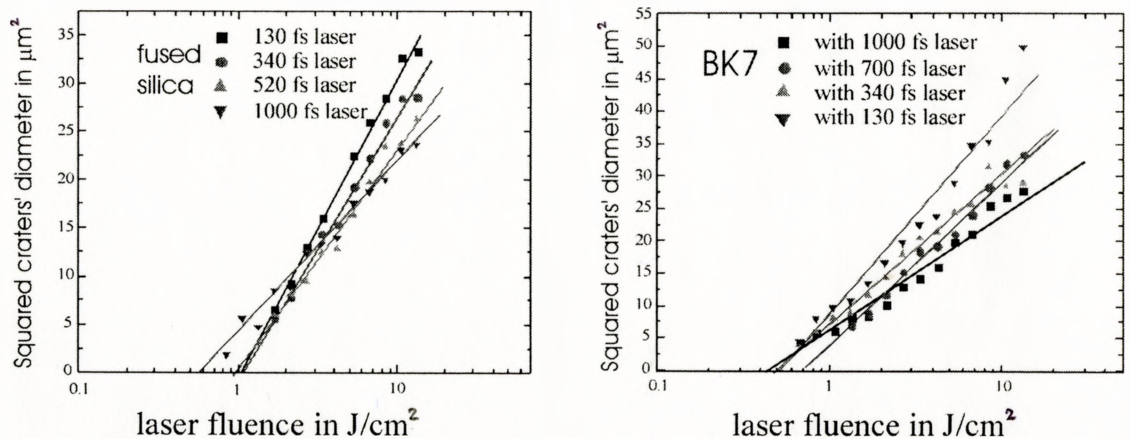

Figure 4.6: Single-shot ablation threshold of fused silica (left) and BK7 glass (right) with ultrashort pulses of different laser durations (from 130 fs to 1000 fs)

The laser ablation threshold in a particular material is dependent on the pulse duration and spectrum besides the intrinsic properties of the target. Some recent publications [19-23] have investigated laser-induced breakdown in optically transparent materials as a function of laser pulse length. Du et al. [20] studied the threshold fluence for plasma emission from fused silica for pulse lengths in the range from 150 fs to 7 ns. They found the expected $\tau^{1/2}$ dependence of the threshold fluence for long pulses (>10 ps). However, for pulse lengths < 10 ps they reported an increase in the threshold fluence with decreasing pulse length. In contrast to Du et al., Stuart et al. [21] and Lenzner et al. [22] did not observe an increase in the damage threshold for pulses <10 ps. In our experiments, we performed 120 fs to 1700 fs threshold damage analysis in fused silica and BK7 glass. Our preliminary result is surprisingly in agreement with Du et al. As shown in Figure 4.5, with single 790 nm laser pulses, the 130 fs laser threshold is ~1 J/cm^2 in fused silica and ~0.51 J/cm^2 in BK7 glass; the 1000 fs laser ablation threshold is ~0.58 J/cm^2 in fused silica and ~0.44 J/cm^2 in BK7 glass. However, the difference is small, the reliability of the experimental result is in the region of ±50%, because of the critical focusing condition, the SEM measurement, spot size measurement, and laser power fluctuation etc. For example, the experimental result we presented in Figure 4.5 that came from another experiment on a different day is different from the result in Figure 4.6. The single-shot (τ=130 fs) ablation thresholds are ~0.64 J/cm^2 in BK7 glass and ~0.79 J/cm^2 in fused silica from Figure 4.5, but here the results are ~0.51 J/cm^2 and ~1 J/cm^2.

The detailed physics of laser ablation with laser pulses in duration from ps to fs is extremely complicated. It is beyond the discussion in this thesis. Interested readers are

referred to references 19, 20, 22, 27. To some extent, this issue is still an unsolved question in laser ablation. Different groups have different opinions. Laser ablation of dielectrics is definitely a good direction for further research.

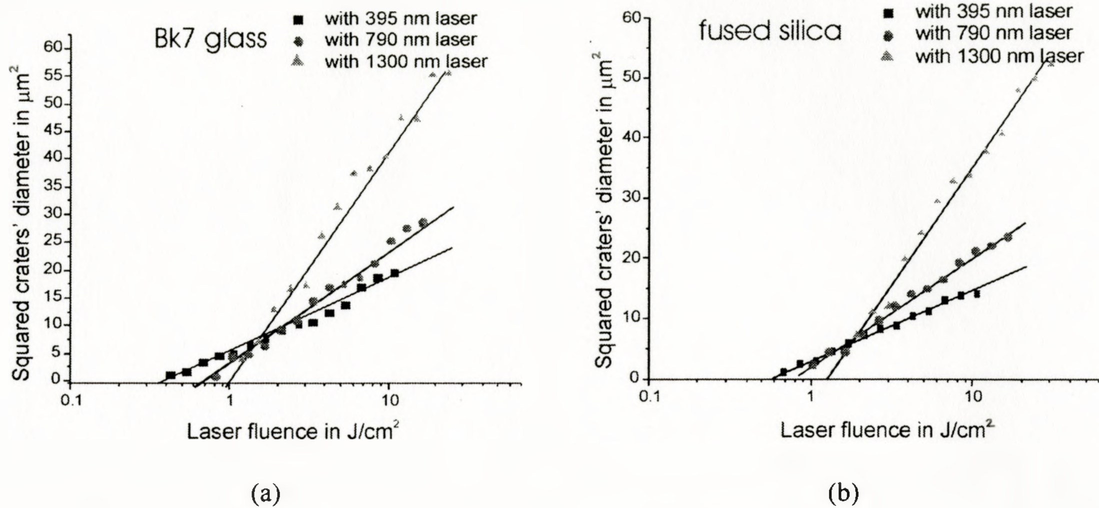

Figure 4.7: BK7 glass (left) and fused silica (right) ablation threshold with different laser wavelengths

The dependence of ablation threshold on wavelength can be due to the frequency dependent photoionization rate. Normally a shorter laser wavelength has a much bigger absorption cross section than a longer wavelength in the spectrum region from 395 nm to 1300 nm. However, from our experiments, there are only small differences (both BK7 and fused silica) in the ablation threshold with 395 nm, 790 nm and 1300 nm light (the calculation of the laser fluence with the 1300 nm laser uses the same spot size as that with 790 nm, so the 1300 nm laser ablation fluence calculation may have bigger error). The reason in part may be that some defects are in the targets so that fewer photons may also excite electrons to valance band, and these free electrons are further accelerated to very high energy so as to induce avalanche ionization in the solid. In addition, some of the literature [18, 22] suggests that multi-photon ionization only generates the electrons

to seed avalanche ionization in ultrashort laser pulses ablation. Therefore, it is not a surprise to see that ultrashort laser pulse ablation threshold is almost independent of laser wavelength.

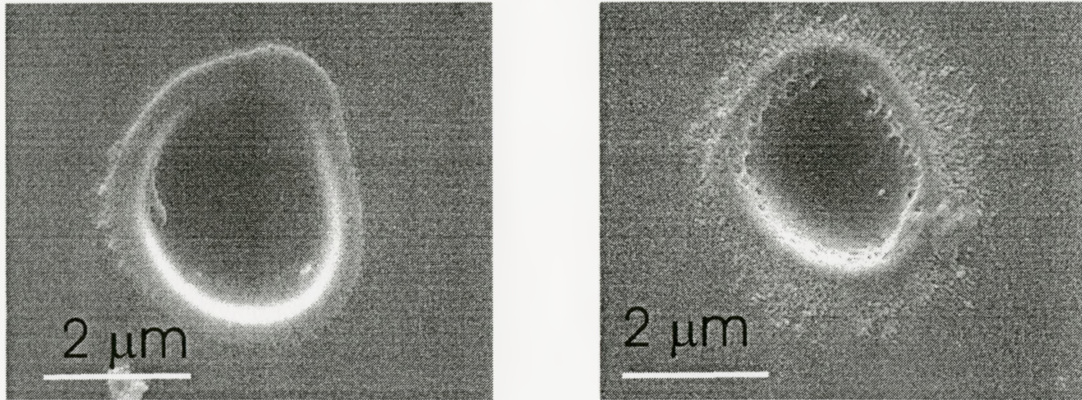

Figure 4.8 (a): (left) Fused silica with 395 nm at fluence 5.8 J/ cm2, (right) BK7 glass with 395 nm at fluence 2.8 J/cm^2

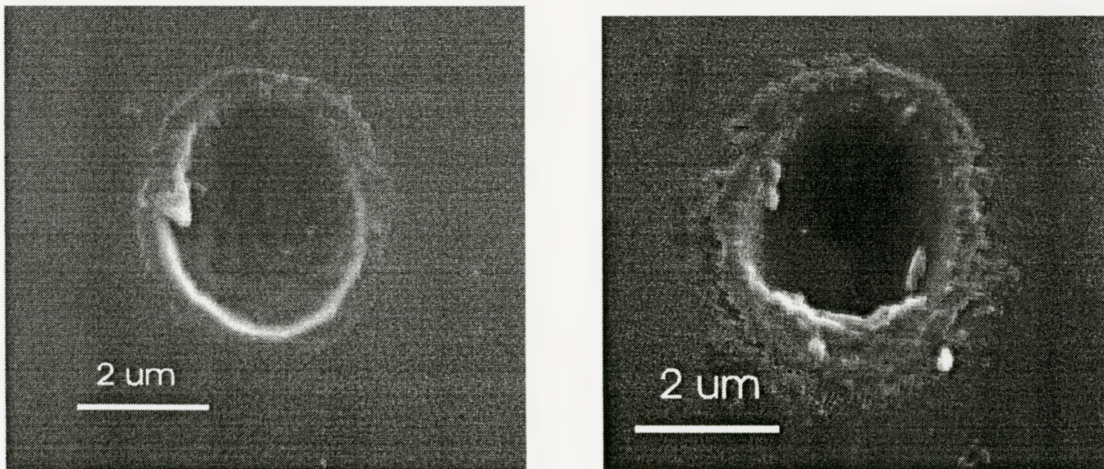

Figure 4.8 (b): Laser ablation of fused silica (left) and BK7 glass (right) at 790 nm with a laser fluence 6.62 J/cm^2

In addition, a shorter wavelength laser can always be focused more tightly than a longer wavelength laser by the same optical lens or optical objective. From our measurement, the 395 nm laser beam has about a 20 percent smaller spot size than the

790 nm laser (Figure 4.9). This means we can induce damage in materials with smaller energy under the case of machining with a shorter wavelength laser than with a longer wavelength laser. So in an experiment, we may feel that a lower energy is needed with a shorter wavelength than a longer one to induce damage in the target. But by calculating the actual laser fluence, we find that the real ablation threshold for 790 nm, 1300 nm and 395 nm wavelengths are very close. This is shown in Figure 4.7 (a) where the ablation threshold for different wavelengths in fused silica is illustrated and in (b) where the ablation threshold of different wavelengths in BK7 glass is shown. Figure 4.8 (a) and (b) are SEM images of single pulse irradiation in fused silica and BK7 glass with 395 nm and 790 nm laser wavelengths. The optical aberrations such as astigmatism from the critical optical alignment make the crater not perfectly circular.

As a Gaussian beam is focused, the transformed Gaussian beam has a variable focusing diameter when the target is put in a different position in the Gaussian beam. The spot size is defined as where the intensity drops to $1/e^2$. We are using a gradient index lens and a 10× objective for micromachining work, and the waist spot size is ~9 μm (see Figure 4.10 a) and ~6.3 μm (see Figure 4.3) respectively. However, by moving the focusing objective back and forth, we can make variable size craters as shown in Figure 4.9 (craters made by gradient lens) with the Gaussian beam that is shown in Figure 4.10. The craters were made by a 130 fs laser pulse (λ= 790 nm, energy: 150 μJ/pulse) in a single-shot pattern.

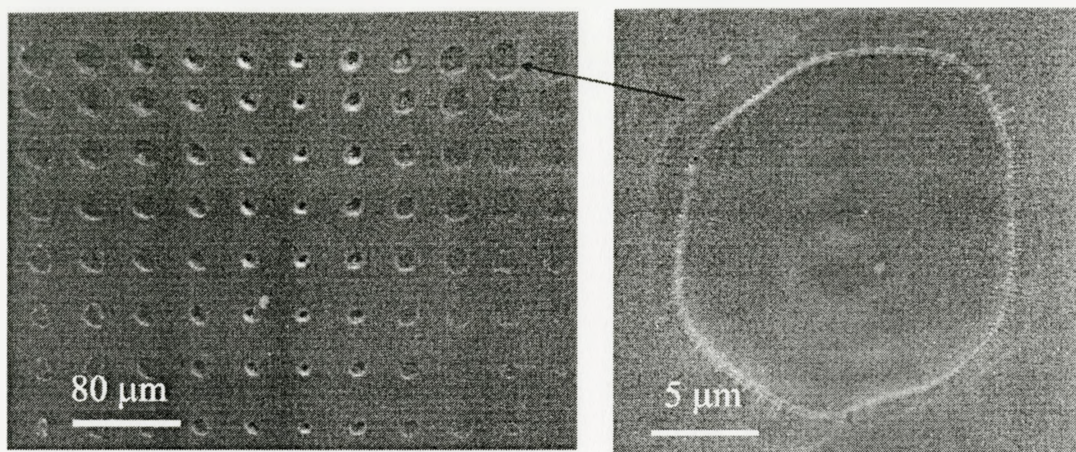

Figure 4.9: SEM images of fused silica surface ablated by single laser pulse (λ=780 nm, τ=130 fs) with energy from 150 μJ/pulse in the first line (top) to 30 μJ/pulse in the last line (bottom), laser focusing was moved down 20 μm in each step in each row (from left to right)

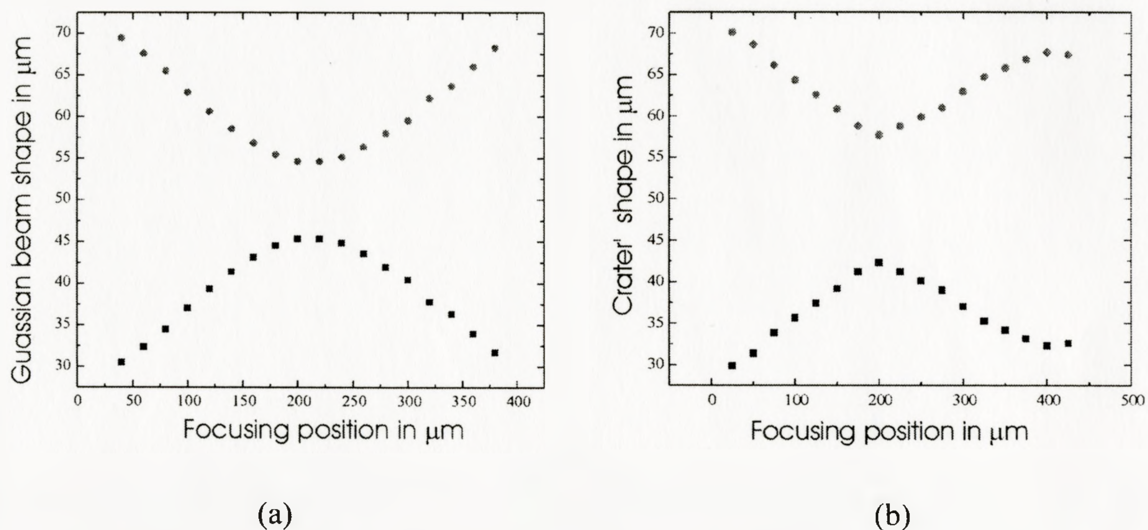

Figure 4.10 (a): Gaussian beam shape focused by gradient index lens

Figure 4.10 (b): Crater sizes in first line of Figure 4.9 with different focusing position

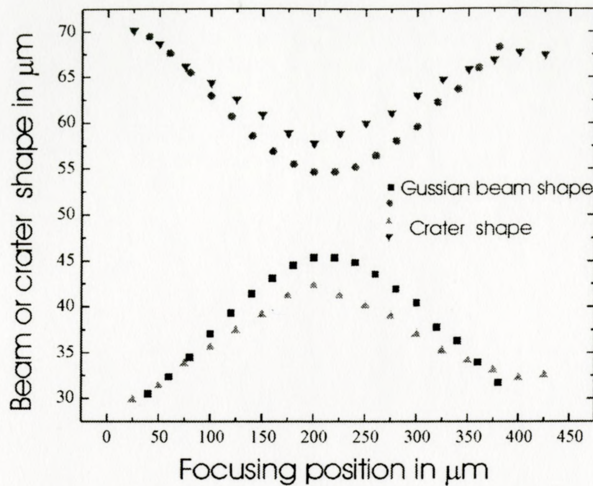

Figure 4.10 (c): Fitting the crater diameters to a Gaussian beam

4.5 Multi-shot Results

The single femtosecond laser pulse induces breakdown or damage in transparent materials due to multi-photon ionization by the short laser pulse. The free electrons from the ionization are further heated, resulting in avalanche ionization and rapid plasma formation [3]. The use of multiple laser shots serves simply to decrease the absolute value of the damage threshold due to incubation effects [13, 18]. We continuously decrease our laser intensity around the single-shot ablation threshold fluence to investigate the incubation effects. Figure 4.11 is an SEM image of a one-shot to ten-shot array in fused silica. We can see an interesting phenomenon. In the first row, which is a single shot sequence, when the laser intensity is low enough (in the left side of Figure 4.11), one laser pulse cannot induce visible damage in material. However, multiple laser pulses do make breakdown in the target as shown in the left corner of bottom in Figure 4.11. This proves the incubation effect does work in femtosecond laser ablation of dielectric materials.

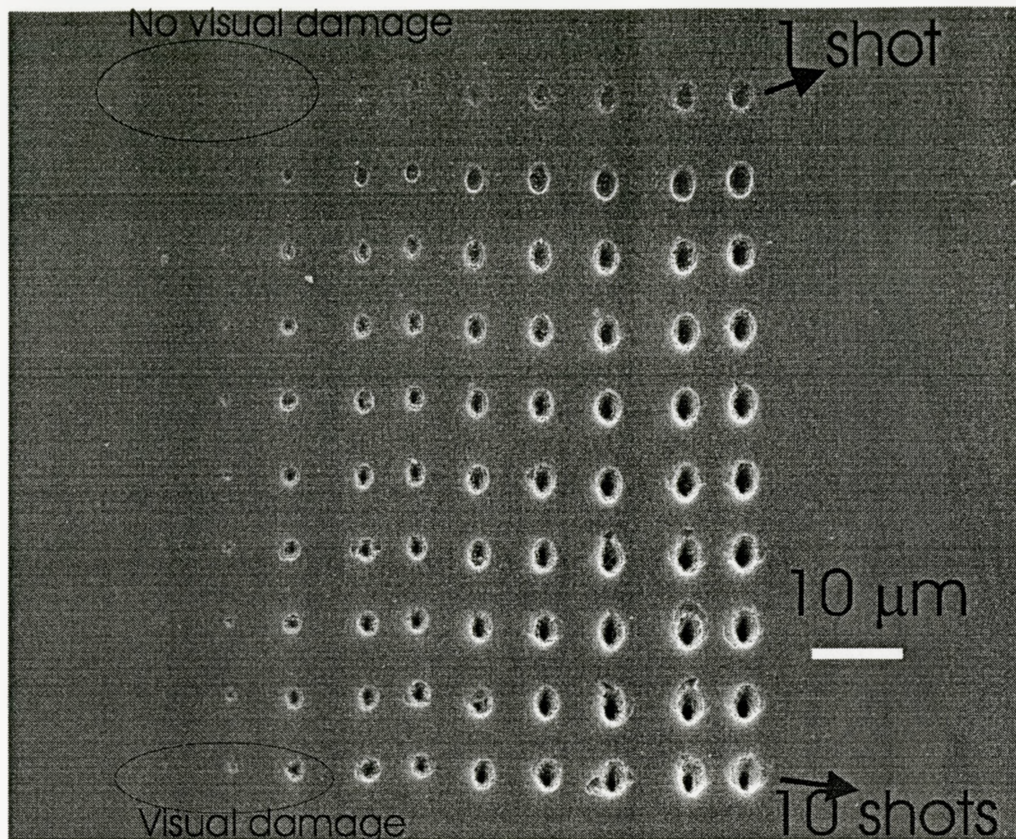

Figure 4.11: Multi-shot pattern in fused silica with laser (τ=130 fs and λ=790 nm) pulse number N=1 (top) to 10 (bottom) at different fluences from high 13.5 J/cm^2 (right) to near threshold fluence 1.35 J/cm^2 (left)

From the report of Campbell el al. [13], the damage threshold decreases by about a factor of two on going from single-shot measurements to multiple-shot (N>100). The incubation effect can be explained by the low-order excitation mechanism from defects close to the surface. An increase in defect concentration with an increasing number of laser shots can occur due to high-order multi-IR-photon excitation of defects [13]. An alternative explanation invokes low-order (one or two-photon) UV-absorption [13]. White light generation or supercontinum generation [31] broadens the spectrum of the incident femtosecond laser pulses when the laser fluence is near the ablation threshold.

So the absorption of the short wavelength components leads to the production of color centers [32]. In our femtosecond laser machining experiments on dielectrics, we did observe the supercontinum effect where visible light is generated when the near threshold ultra-short pulses (λ=790 nm) interact with the surface of the dielectric target.

We investigated the evolution of surface features in materials ablated by single and multi-shot femtosecond laser pulses. Under multi-shot irradiation, the roughness of the target is expected to increase based on other results in the literature [18]. The rim in the feature of Figure 4.12 (a) which is after single-shot ablation by a femtosecond laser pulse has been melted and should have some defects. These defects or color centers then serve as the absorption center for the second femtosecond laser pulse. Therefore, the region in the rim exhibits more absorption than other regions, so it will be removed to a greater extent with the second pulse. This is the reason why the feature made by two shots is in so good symmetry with the first shot crater.

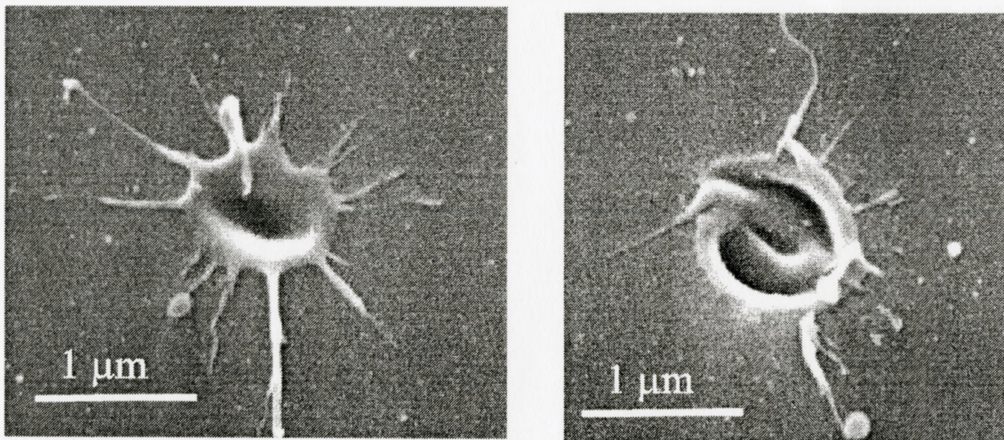

Figure 4.12 (a): Laser ablation in zinc titania glass with laser (τ=130 fs and λ=790 nm) pulse number N=1 (left) and N =2 (right)

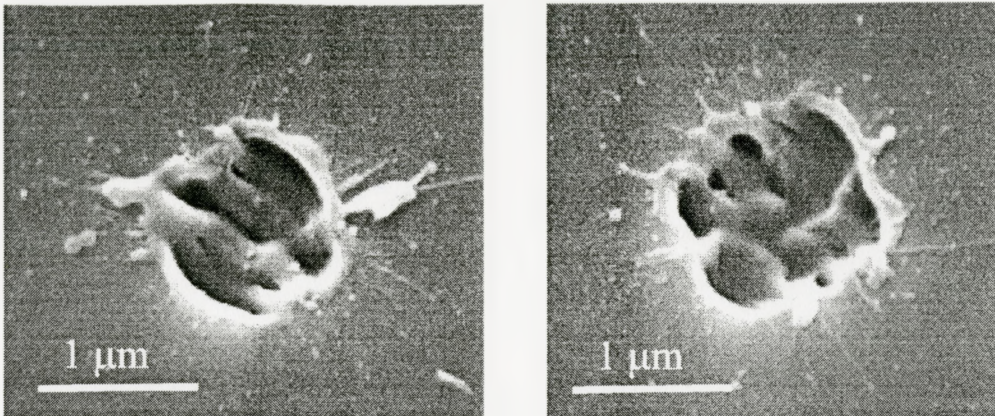

Figure 4.12 (b): Laser ablation in zinc titania glass with laser (τ=130 fs and λ=790 nm) pulse number N=3 (left) and N=4 (right)

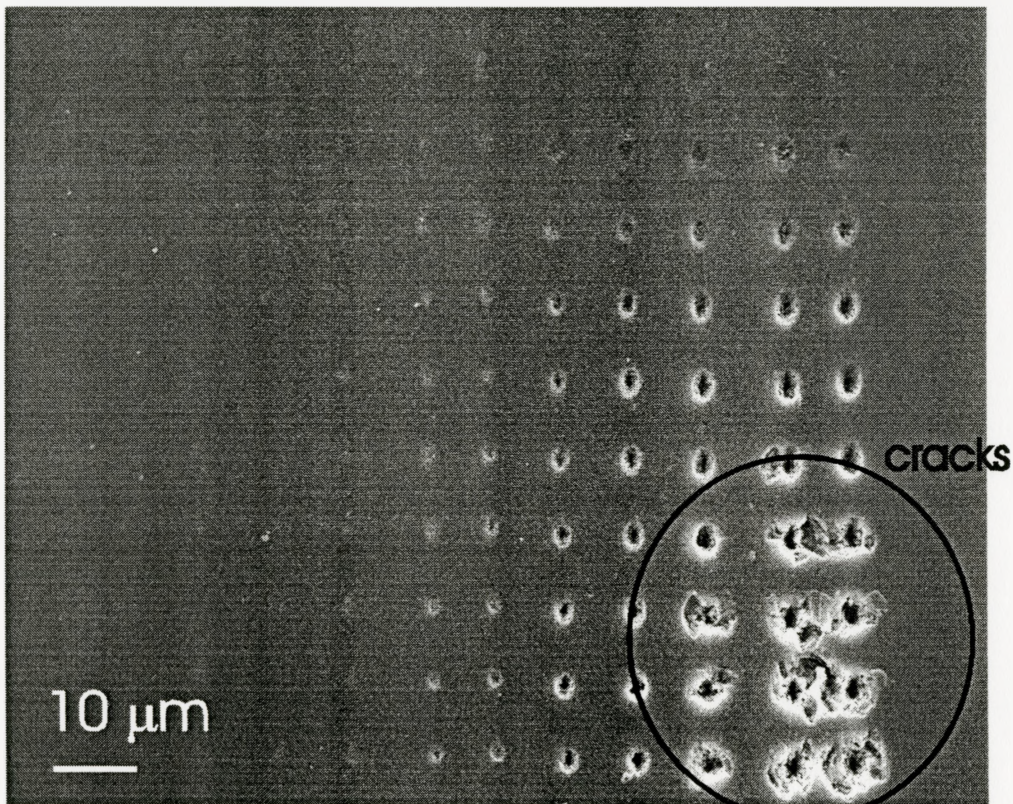

Figure 4.13 (a): Multi-shot pattern in fused silica at laser duration 1700 fs with laser (λ=790 nm) pulse number N=1 (top) to 10 (bottom) with step-attenuated fluence from right side to left

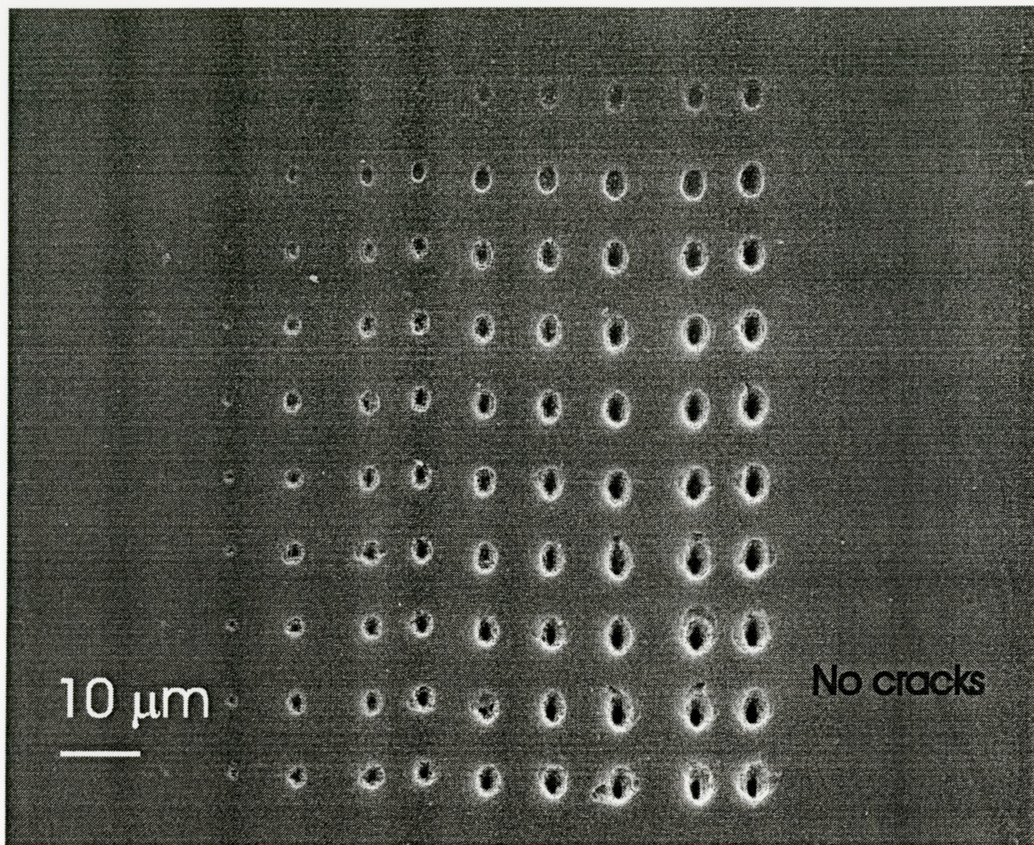

Figure 4.13 (b): Multi-shot pattern in fused silica at laser duration 130 fs with laser pulse (τ=130 fs and λ=790 nm) number N=1 (top) to 10 (bottom) with step-attenuated fluence from right side to left

We also found that laser pulses of shorter duration are more controllable than longer ones in material removal which is in agreement with E.E.B. Campbell group [18]. From the Figure 4.11, which is done with 130 fs laser pulses, the ablation region is controllable. On the contrary, with a longer pulse (1700 fs), the multi-shot pattern appears broken and cracked (see Figure 4.13 a). We observed the same effect in fused silica and BK7 glass. The fluence was controlled to be the same in the two cases (130 fs and 1700 fs), ~4.2 J/cm^2 before being attenuated by neutral density attenuators from OD 0.04 to

OD 2.4. From Figure 4.13 (a) multi-shot irradiation with 1700 fs pulses and (b) multi-shot irradiation with 130 fs, we are able to say that for long pulse ablation the high temperature electrons do penetrate into the dielectric target and induce avalanche ionization in wide area to induce a cracking or breaking effect. Extensive studies should be conducted on the defect analysis based on detailed TEM evaluation of the residual material after single-shot and multi-shot irradiations.

4.6 Potential Applications

4.6.1 Biochemical Sample Holder

The biochemical industry needs smooth and shallow craters in glass or other dielectric materials to confine biochemical samples (as shown in Figure 4.14) such as proteins and DNA for photoluminescence analysis. The craters are supposed to be relatively smooth and shallow in diameter (~50 μm and below). It is hard to make such feature in glass, which is brittle, with traditional nanosecond lasers. The thermal diffusion and the relatively large amount of energy induce cracking and breaking as shown in Figure 4.1 (a big cracked crater made by a nanosecond laser). Certainly, the deep UV excimer lasers may do this job well. However the thermal diffusion still will potentially induce some defects or lead to damage around the crater, which is undesirable for photoluminescence experiments. Further investigation should be done on this via TEM and photo-luminescence studies. Another way to fabricate the craters for this purpose is through chemical etching that is widely used in the semiconductor industry, as discussed in chapter 2. But the complicated processing will raise the product's price very much. Another way is via femtosecond laser micromachining. We can use single laser pulses to

induce such structures in glass. So far we made craters (diameter < 40 μm which is limited by the laser power) in fused silica, BK7 glass, fused quartz and zinc titania glass.

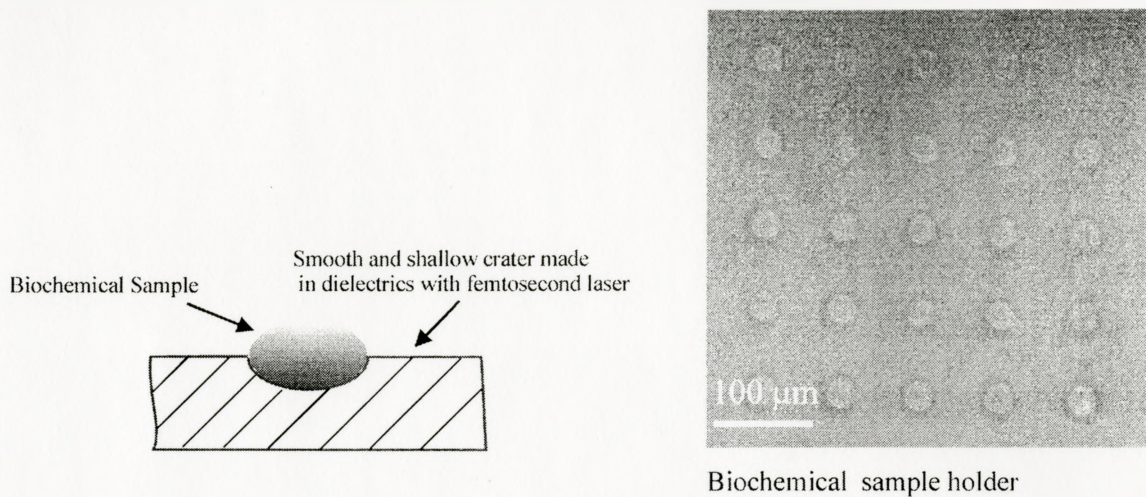

Figure 4.14: (left) Biochemical sample is held in a smooth crater, (right) crater array fabricated in fused silica working as biochemical holder

The reason why we used single-shot irradiation to induce craters rather than multiple-shot irradiation is that the crater induced by a single laser pulse is smoother than the one induced by multiple laser pulses. Also, in the single-shot ablation approach, the work is time saving and efficient. We can increase the productivity with higher speed motors. For example, our laser could be adjusted to repetition rates as high as 1 kHz, so by fast scanning, we can make 1000 craters in one second. Let us suppose that a biochemical sample holder plate has a 100×100 crater array; in that case we would need around 10 seconds to make it. In one hour, we would fabricate 360 plates. If we have enough energy in the future to split one laser beam to two or more, the efficiency will be correspondingly increased.

4.6.2 Photonics Components Processing

Transparent glass materials provide the backbone of many of today's rapidly expanding photonics application areas, which serve such diverse fields as optical communications, electronics, sensor technologies, medicine, and materials processing. For optical communications, this means the development of planar lightwave circuits that combine directional couplers, add/drop filters, multiplexers, switches, wavelength converters, attenuators, and more onto a single chip.

The future evolution of photonics will be dictated by the development of precise processing tools that can nano-structure optical materials [33]. Such devices are used to alter and control the pathway of light in optical systems. Feature sizes only a small part of an optical wavelength, i.e., ~100 nm for $\lambda/10$, are required for critical dimensions. One approach to processing includes the direct shaping of optical surfaces by micromachining or etching. Alternatively, refractive index changes [34] can be patterned internally in optical materials as is currently done in fabricating fiber Bragg gratings with ultraviolet lasers. For many of these applications, fused silica is the preferred material, providing high transparency, and stable properties over long lifetimes and at high temperatures. However, these ideal properties also present a challenge in materials processing, especially on the scale of 100-nm feature size. With femtosecond laser pulses, people can induce sub-micron surface structures such as gratings by a two-beam holographic method in dielectric materials such as $LiNbO_3$ [35]. Surface relief gratings have been achieved in a variety of transparent dielectrics, including Al_2O_3, TiO_2 and SiO_2 glass with some approaches [36]. In addition, laser beam direct writing for fabrication of waveguides can be realized with ultrashort pulse lasers [37].

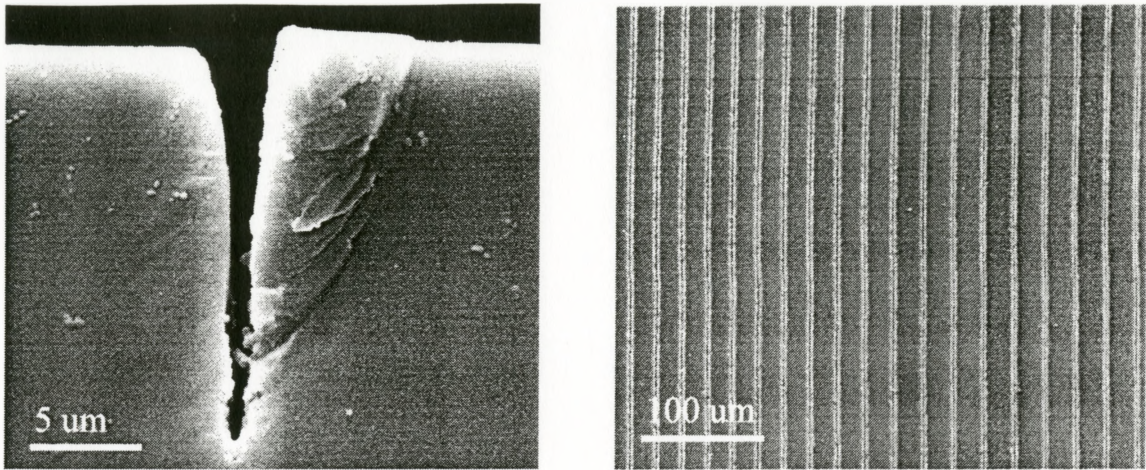

Figure 4.15: Ti: sapphire laser cutting trench (left) and gratings (right) in dielectrics

Laser materials processing is widely employed by the electronics industry today for trimming components, patterning the smallest features in critical layers of silicon ships, etching structures, circuit repair, and metal-conductor deposition. However, because of the high transparency of fused silica, current industrial laser systems interact weakly with glass, and do not provide the control required in shaping optical devices. We can use 790 nm laser beams and frequency doubled 395 nm femtosecond laser pulses to machine features (see Figure 4.15) in dielectric materials. The interesting point for femtosecond laser micromachining is that the damage region can be controlled to be smaller than the diffraction limit. So we can make small features close to λ with a simple $10\times$ objective. In addition, with nonlinear optical techniques, such as frequency doubling, frequency tripling and frequency mixing, people can convert the near-IR femtosecond laser pulses to deep UV. Femtosecond lasers will probably take the place of the excimer lasers in the laser processing industry. Femtosecond lasers can induce large refractive index changes inside optically transparent materials via the multi-photon adsorption. Now, the fiber Bragg grating industry are using excimer lasers, and normally the

refractive index change is as small as 10^{-5}. With femtosecond laser pulses, the refractive index may be increased to ~10^{-3} region [34]. Then, the fiber Bragg grating can be made shorter and the fabrication takes shorter time; therefore it becomes more economical.

Above all, with femtosecond laser pulses, we can induce high aspect ratio holes, and fabricate gratings or waveguides in dielectrics materials. They are potential applications for the microelectronics and photonics industries. Further defect analysis by detailed TEM evaluation and selected optical analyses of dielectrics after femtosecond laser micromahcining is needed in future work.

Chapter 5. Femtosecond Laser Ablation of Metals

5.1 Introduction

It is well known that metals are very problematic materials for micromachining with lasers owing to their high thermal conductivities and high melting temperatures. With conventional lasers delivering pulses longer than 1 ns, the ablation of metals is always accompanied by the formation of large heat-affected zones and an expulsion of molten material. This limits the achievable precision and the quality of the produced structures.

A significant improvement in this field has become possible because of ultrashort pulse lasers. With ultrashort-pulse laser systems, measurements of laser-induced damage and ablation thresholds on metals have already been performed for both a very broad range of pulse durations and wavelength regions. Comprehensive ablation experiments of metals such as Cu, Al, Fe, Au, and Ag by using solid state femtosecond lasers and excimer lasers have been reported [38-42], where laser fluences range from 0.1-10 J/cm^2 and pulse widths extended from 20 fs to the nanosecond scale with wavelengths from the UV to near IR [41].

By using a femtosecond ultraviolet excimer laser, Preuss et al. [41] found that the ablation threshold of metal thin films on a fused silica substrate was reduced by two orders at 248 nm (τ=500 fs). This result means that the thermal diffusion process is of importance for materials that have relatively high thermal conductivity. They also think that the development of high intensity ultraviolet femtosecond lasers is very likely for laser materials processing [41].

Ablation experiments on metals by using solid-state Ti:sapphire lasers have been reported [39, 42]. X. Zhu et al. [39] reported experimental results of drilling micro holes in Al, Mo, Ti, Cu, Ag, Au, and brass thin metal foils using Ti:sapphire laser pulses (laser durations: 60 fs, 50 ps and 10 ns). Metal ablation threshold and surface morphologies are both discussed. They found the ablation thresholds of different metals are closer when they are ablated with fs laser pulses than with ps and ns laser pulses. Comparison of hole drilling using femtoseond pulses with ps and ns pulses indicates a significant melting is present in both ps and ns regimes, however, with fs pulses, fewer and much smaller droplets around the ablated features are observed. Therefore, it proves that fs laser machining is evidently more advantageous than ps and ns machining for hard materials and deeper hole drilling.

K. Furusawa et al. [42] studied the fs ablation of Au, Ag and Cu with laser pulse widths ranging from 120 fs to 800 fs. They found two different ablation regimes in terms of the laser fluence. The two ablation regimes are discriminated by the amount of particles accumulated by the ablation process. Ablated particles were less in the lower fluence regime than in the higher regime. They believe that the ablation depth is dependent on the thermal diffusion length in the case of high-fluence ablation; and in low-fluence ablation, the ablation depth is dependent on optical absorption skin depth ($1/\alpha$). They also illustrated that the ablation threshold is gradually reduced with decreasing pulse width (in the range of 120 fs to 800 fs).

Lawrence Livermore National Laboratory [40] observed the morphology of the hole's bottom has a dependence on fluence, number of shots, and polarization during the evolution of the hole-drilling. They used a very powerful Ti:sapphire laser system (120

fs, 6 W average power at 1 kHz, λ=825 nm) to drill ~300 μm diameter holes in stainless steel, nickel alloy, and aluminum. They observed that the roughness of the bottom of the holes increases as the laser fluence or number of laser shots increases.

The main motivation of our work on laser ablation of metals was to investigate the surface evolution in metals with femtosecond ablation in comparison with the literature discussed in former paragraphs. In particular, we want to explore via SEM and TEM analysis what has happened to the material after being laser irradiated. In our lab (Photonics Research Laboratory), we have done extensive work on femtosecond laser ablation of semiconductors based on SEM, AFM and TEM analysis [30]. So far, in the research of ultrashort pulse laser micromachining, a lot of work has been reported on how to cut and drill efficiently, and how small features people can make in metals. However, few reports have talked about the difference between the femtosecond laser ablation of metals and semiconductors. We performed single-shot and multi-shot laser pulse irradiation of metals and analyzed the samples with SEM, AFM and TEM to obtain both the surface detail and the material lattice information. We found the surface morphologies in metals after laser ablation are much different from semiconductors, and different metals have different ablated surface morphologies as well, see Figure 5.1 (single-shot irradiation of metals and semiconductors). The preliminary TEM result shows boundary and sub-boundary defects in single-crystal Cu after laser irradiation.

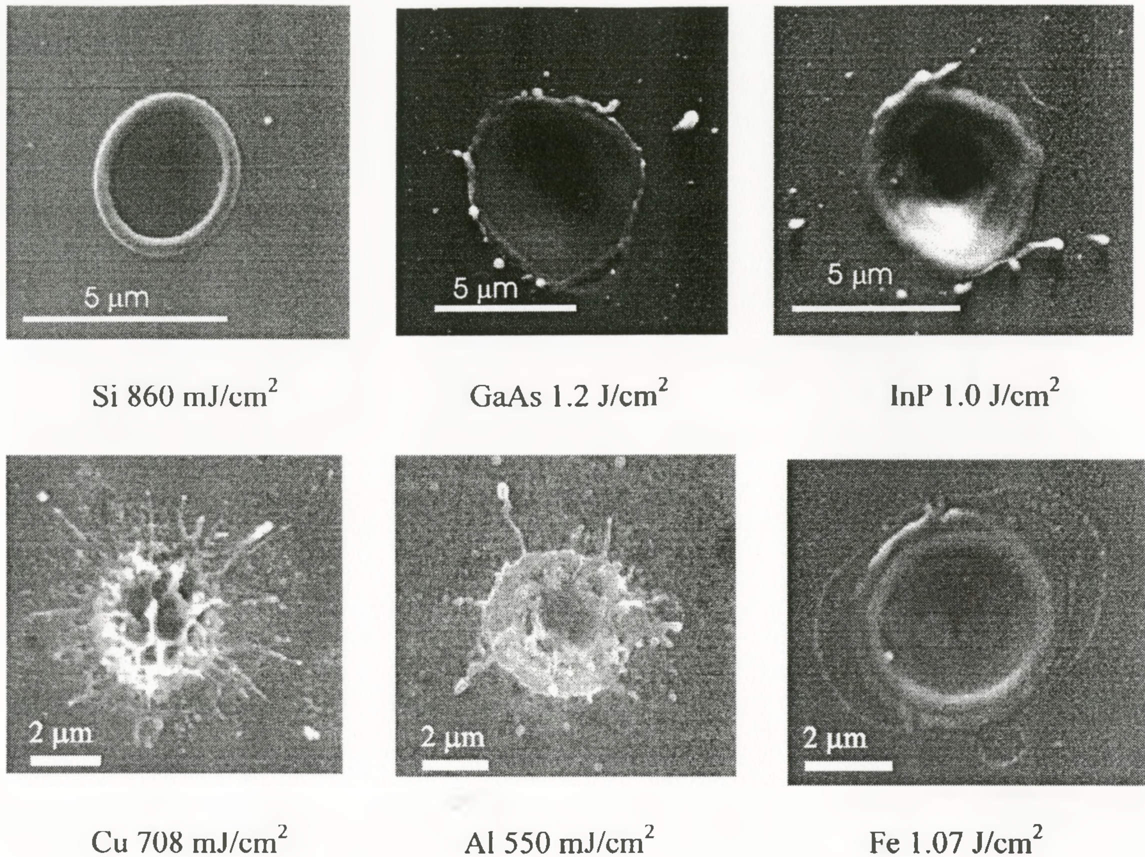

Figure 5.1: Single-shot irradiation of semiconductors (Si, GaAs, and InP) (SEM images from A. Borowiec) and metals (Cu, Al, and Fe) at specified laser fluences at a wavelength of 790 nm

5.2 Experimental

The laser system used in this work was also the Spectra Physics system that was used for ablation of dielectrics. Single crystal Cu, Fe, Al and poly-crystal Cu, Fe, Al are investigated via femtosecond laser pulse ablation. Samples were mechanically polished (roughness < 1 µm) and spark-cut into proper size, normally a D=3 mm disk which is a proper sample for SEM, AFM, and TEM.

5.3 Single-Shot Results and Discussion

With SEM, we measured the diameters of craters induced by femtosecond pulses for laser wavelengths of 790 nm and 395 nm and for different laser intensities. By using the same approach as in the dielectrics threshold analysis we can fit the D^2 of features in metals to laser fluence, and the fluence at $D^2=0$ is the ablation threshold. As shown in the Figures 5.2, the ablation threshold in Cu (poly-crystal) is ~0.09 J/cm^2 with a wavelength of 790 nm and ~0.04 J/cm^2 at 395 nm. The ablation threshold in Fe (poly-crystal in α phase) is 0.04 J/cm^2 at 790 nm and ~0.02 J/cm^2 at 395 nm light. Ablation of metals with UV light has a lower ablation threshold than in the IR. The widely accepted reason is that the absorption cross-section in metal is larger for shorter wavelengths than for longer wavelengths. But the difference from our experiments is small.

The ablation threshold with a 130 fs laser pulse (λ=790 nm) on Cu is relatively low compared to some other publications [38, 42]. S. Nolte et al. [38] reported $\phi_{th}^{(1)}$=140 mJ/cm^2 which is close to our result of 90 mJ/cm^2. However, K. Furusawa et al. [42] suggested a much higher ablation threshold of 430 mJ/cm^2 for Cu with a laser pulse of λ=790 nm, τ=120 fs. A few possibilities may explain the difference. First of all, the Cu sample's roughness in different groups may be different. Roughness will affect the reflectivity of the sample surface; therefore the absorption rate may be different. Secondly, we may have made a mistake in the laser pulse energy measurement or spot size measurement. The third possibility is that we are using different model to S. Nolte et al. and K. Furusawa et al. They obtained the threshold in Cu via the relationship between the ablation rate/ablation depth and laser fluence for Cu target, however, we used the lateral dimension/diameter of the ablated crater versus the laser fluence. In particular in

the case of metals, the exact diameter of the crater is hard to determine due the melting and splatter. So observing a difference is not a surprise. In the near future, we will get smoother metal samples (roughness <10 nm) by electrical or chemical polishing. With these improved samples, we can compare the threshold results from the model that S. Nolte at al. and K. Furusawa et al. used with the one that we have used in this thesis.

Another point worthy of mention is that S. Nolte at al. and K. Furusawa et al. both reported the ablation thresholds for two ablation regimes. S. Nolte et al reported $\phi_{th}^{(1)}$=140 mJ/cm^2 and $\phi_{th}^{(2)}$=460 mJ/cm^2 in poly-crystal Cu. Although we don't have any solid proof to show this phenomenon in Cu or Al ablation at present, we believe that it is partially because our fluence has not been extended sufficiently high to show this effect clearly. We do find some clue of second ablation regime in single-crystal Fe ablation experiment which will be discussed in part 5.4.

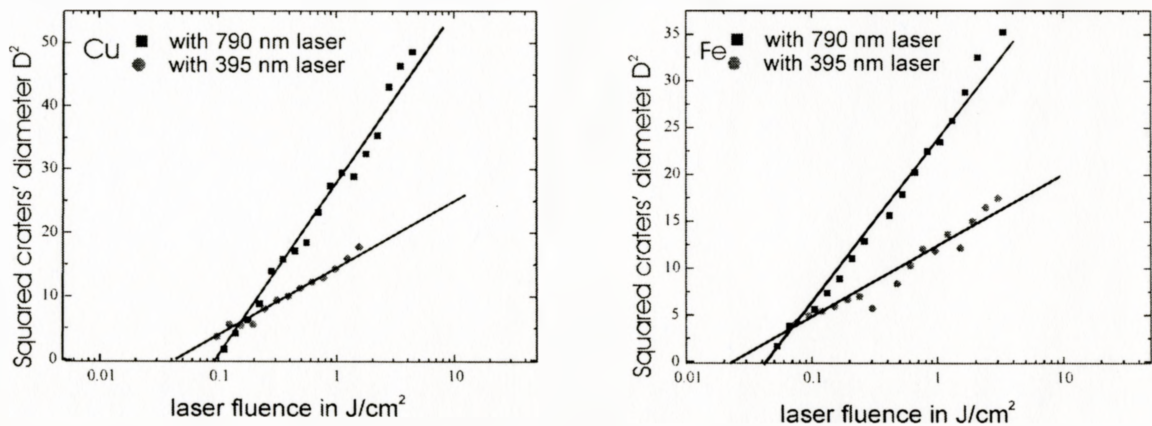

Figure 5.2: Squared diameters D^2 of the ablated craters in Cu (left) and Fe (right) with single laser pulse (τ=130 fs, λ=790 nm and 395 nm) as a function of the laser fluence

Figure 5.1 shows SEM photographs of single-shot irradiation on semiconductors (Si, GaAs, and InP) and metals (Cu, Fe, and Al). We can see that the surface morphologies are much different. In high thermal diffusivity materials such as Cu

(thermal diffusivity is 113 cm^2/s) and Al (thermal diffusivity is 91 cm^2/s), the ablation surface is very rough and even swells up. As discussed in the literature [43], the heat exchange between the molten zone and the surrounding material proceeds well after the laser pulse is over. The process will proceed very fast in case of high thermal diffusivity (Cu and Al). Then the vaporization recoil can expel the thin fluid layer violently. So in our case, the surfaces of Cu and Al samples which have high thermal diffusivities look very rough and violent, but for semiconductors (thermal diffusivity Si: 0.8 cm^2/s, GaAs: 0.31 cm^2/s, InP: 0.372 cm^2/s) which have relatively much lower thermal diffusivities, the solidification of the fluid is slower, so that the smooth surfaces are achieved via the surface tension in the liquid phase. Fe, with a thermal diffusivity of 21 cm^2/s which is relatively lower than in Al and Cu, has a clear crater structure after single-shot irradiation, but the crater does not look as good as those in semiconductors which have much lower thermal diffusivity.

The absorption of 395 nm or 790 nm laser light in metals is in a very thin layer, about 10 nm (13 nm thick in Cu with 790 nm laser) because the large amount of free charges in metals [43]. However, from the profile of the crater from AFM analysis of metal ablation shown in Figure 5.3, we can see that the real ablation depth is far deeper than 10 nm. At a medium fluence of 1.7 J/cm^2, the depth is ~ 500 nm as shown in Figure 5.3 AFM images of single shot irradiation of a Cu crystal. In nanosecond laser machining, the thermal diffusion can explain the deep ablation.

This is a good question for femtosecond laser machining. We think one reason is still the thermal conductivity. From the thin film ablation threshold experiment of S. Preuss [41], the ablation threshold of a thin film is dependent on the thickness; this result

means that the thermal diffusion process is of importance for materials that have relatively high thermal conductivity. The second reason may be the phase explosion induced by high pressure [44] in the case of high or medium fluence ablation in which the phase explosion is very serious, and the pressure from the explosion ejects the melted layer off the target.

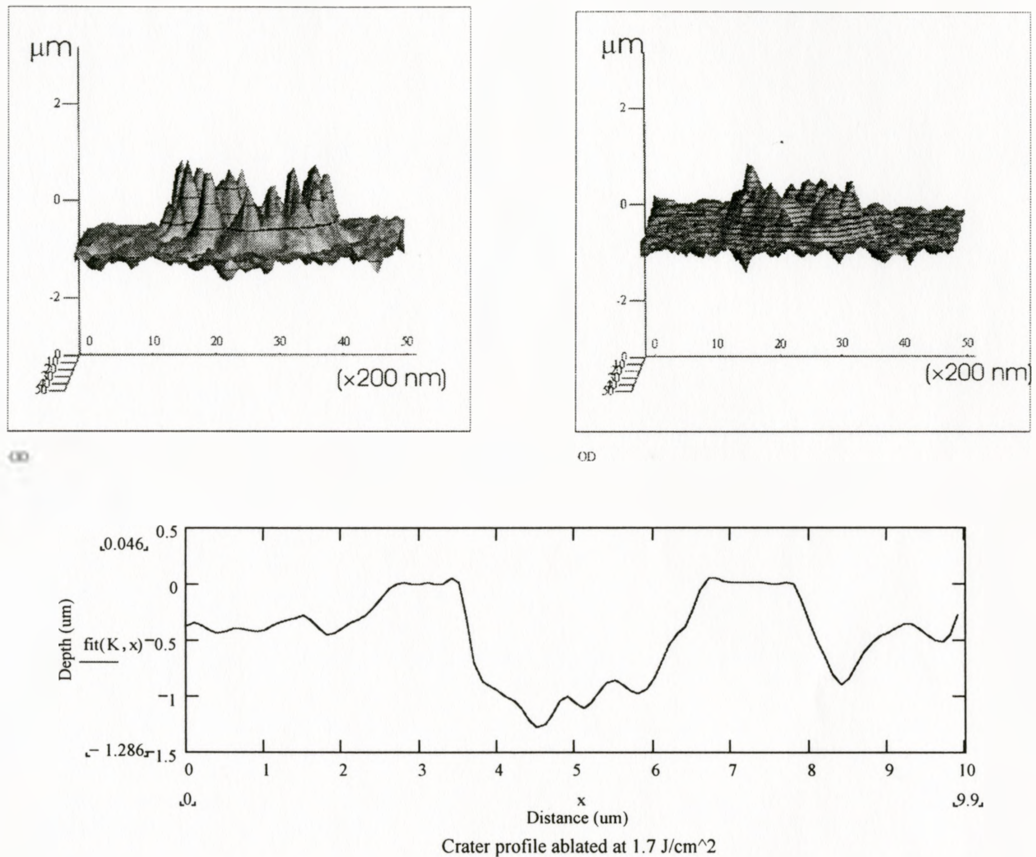

Figure 5.3: AFM images of single-shot irradiation of Cu single-crystal with fluence 1.7 J/cm^2 (upper-left) and 0.86 J/cm^2 (upper-right), and (below) the profile of the crater ablated with laser fluence 1.7 J/cm^2

In the publication of K. Furusawa et al. [42], they presented that the ablation depth is dependent on the thermal diffusion length at higher fluence (fluence over 3 J/cm^2 for Cu), and is dependent on optical penetration length at lower fluence (< 0.4 J/cm^2 for

Cu). In our experiments, it was hard to get the depth resolution less than 100 nm with AFM because the mechanically polished samples' roughness is larger than 100 nm. So, in order to see the precise ablation depth at lower fluence, better metal samples which have a roughness <10 nm are needed. We should be able to get a better surface on the sample by using electrical polishing or chemical polishing after 1 μm mechanical polishing. With a smooth sample, we can investigate the ablation depth with improved precision. At the same time, the defects in the surface that are induced by mechanical polishing will be reduced a lot in the single crystal metals by using electrical polishing and chemical polishing. The reduction in the concentration of defects in the sample's surface will improve not only the investigation of the ablation threshold in metals but also the TEM analysis. The first TEM result shows defects in the ablation region, however sample polishing could be another possibility for inducing these defects in the single crystal Cu sample besides laser ablation.

Figure 5.4 shows TEM observations of laser ablated Cu single crystal after ion milling. The laser irradiation utilized 5 μJ pulses in single-shot pattern. Figure 5.4 (a) shows a small hole obtained by the ion milling process. The hole is smaller than 4 μm across. The area shown in the figure 5.4 (a) is located in the central part of the laser-produced crater. Figure 5.4 (b) shows a bright field TEM image indicated by the arrow in the figure 5.4 (a). We can see a discontinuity of contrast, indicated by arrows. Figures 5.4 (c) and (d) show selected area electron diffraction patterns corresponding to region A and region B in the bright field image, respectively. The diffraction pattern of figure 5.4 (c) means that vertical vector of the region A is [011]. The figure 5.4 (d) means that vertical vector of the region B is [-114].

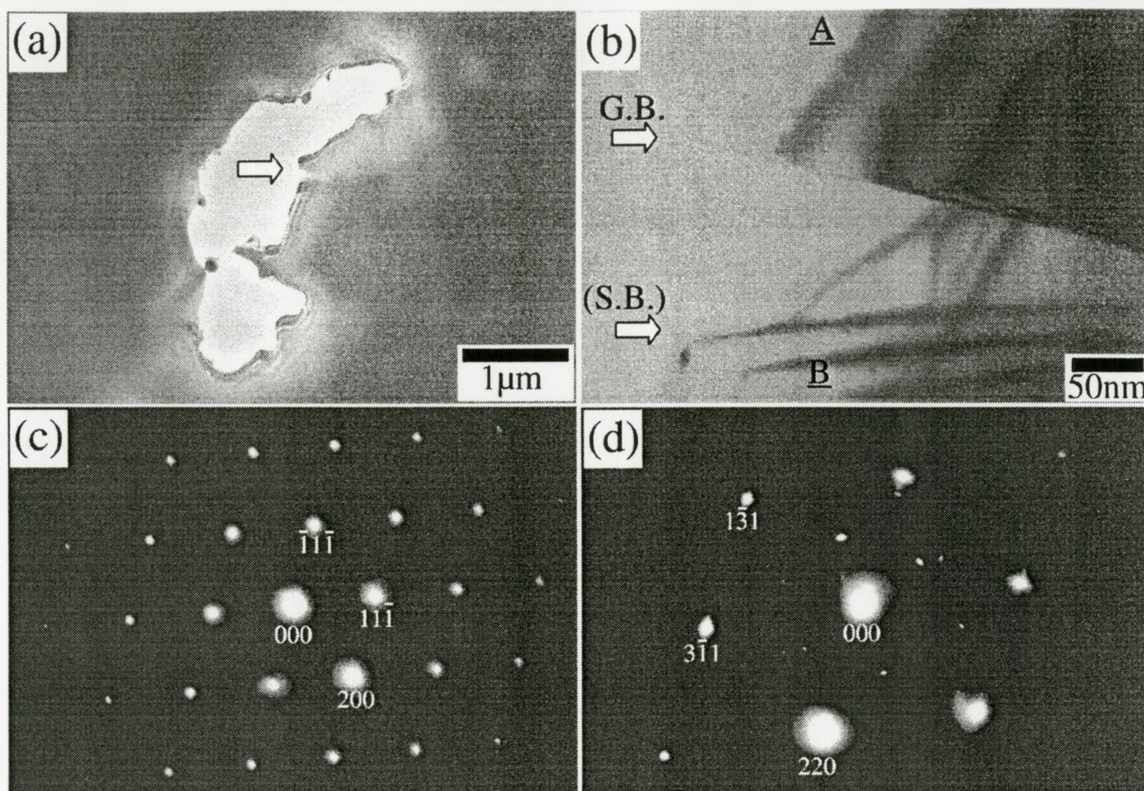

Figure 5.4: TEM observations of Cu single crystal after 5 μJ single pulse laser irradiation. (a): TEM image of laser irradiated Cu single crystal after ion milling. This area is located in the central part of the laser-produced crater. The arrow shows the position, which corresponds to the following micrograph, for detailed observation. (b): Bright field image around the boundaries. The arrows show the position of grain boundary and sub- boundary. (c): Selected area electron diffraction pattern corresponding to the region A in the bright field image (b). (d): Selected area electron diffraction pattern corresponding to the region B in the bright field image (b) (TEM images provided by Junji Yamanaka)

From these TEM results, we can conclude that there is a grain boundary between regions A and B as pointed in the figure 5.4 (b). Probably, there is also sub-boundary as pointed in the figure 5.4 (b). We did not take diffraction patterns of the narrow area between the two arrows in the figure 5.4 (b). However, we believe that there is a sub-boundary from the shape of thickness fringes.

The grain boundary and sub-boundary introducing process can be considered as follows. A small amount of Cu was melted during the radiation. Then new Cu crystal grew on the remaining part of the single crystal Cu. However, the growth mode was not layer-by-layer growth and there may be many nucleation sites. Most of all melt grew epitaxially, but some of them did not grow epitaxially. Hence, grain boundaries or sub-boundaries were introduced. The region around the crater induced by fs laser pulse should be studied via TEM as well to show if the thermal effect induces defects or not.

5.4 Single-Shot Ablation of Poly-crystal Fe and Single-crystal Fe

We used both poly-crystal metals and single-crystal metals in femtosecond laser ablation experiments. Initially, the purpose of using single-crystal metals was for the TEM analysis. However, the preliminary results from laser irradiation of Fe via SEM show that ablation in these two kinds of materials is fairly different, including the quantitative aspects of the ablation threshold and surface morphologies.

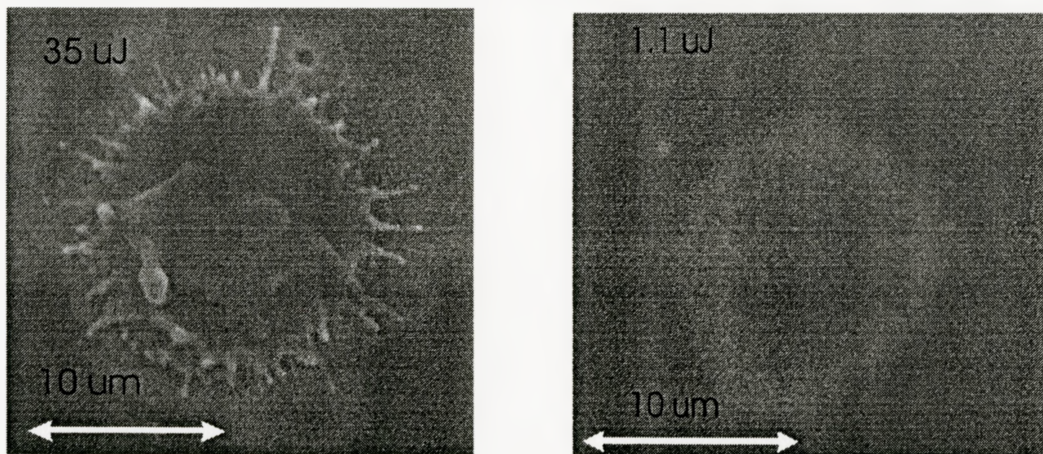

Figure 5.5 (a): Fe single-crystal single-shot ablation with high (113 J/cm^2) and medium (3.5 J/cm^2) fluence

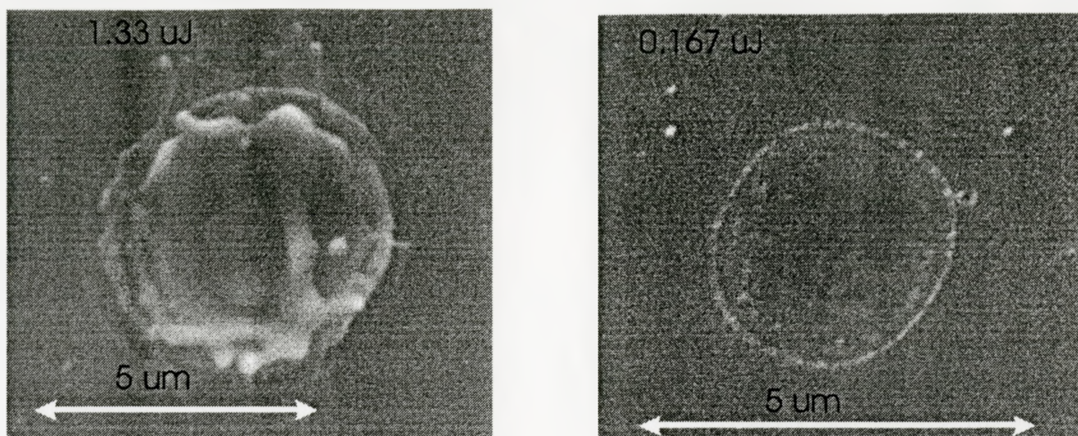

Figure 5.5 (b): Poly-crystal Fe single-shot ablation with medium fluence (4.3 J/cm^2) and low fluence (0.54 J/cm^2)

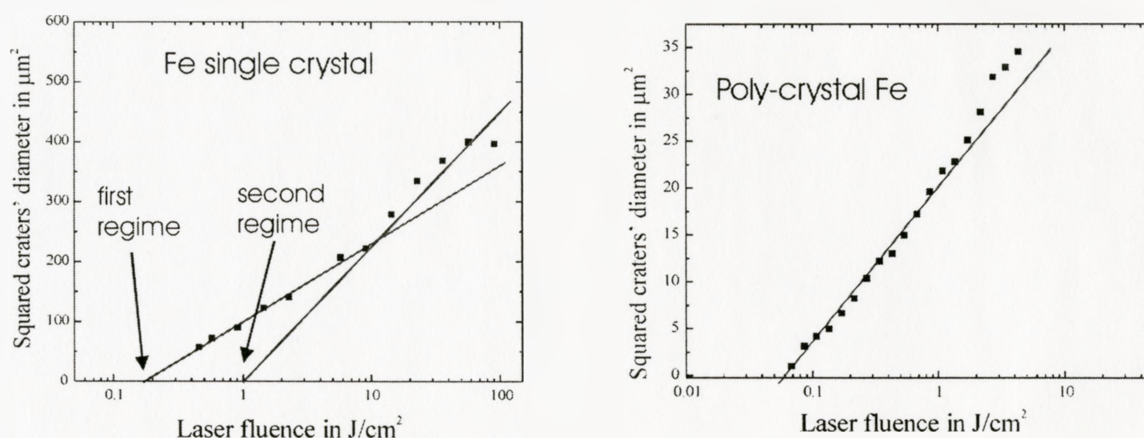

Figure 5.6: Squared diameter D^2 of the ablated craters in single-crystal Fe (left) and poly-crystal Fe (right) with single laser pulse (τ=130 fs, λ=790 nm) as a function of the laser fluence

Figure 5.5 (a) and (b) are SEM photographs of poly-crystal Fe and single-crystal Fe samples respectively. We can see in Figure 5.5 (b) that with ~1.3 µJ/pulse, we can induce a nice crater in poly-crystal Fe metal. However, there is no crater structure at all with this fluence in single-shot pattern in single-crystal Fe. Also, by fitting the squared diameter of craters to laser fluence, as shown in Figure 5.6 we determined the thresholds

in these two different materials. The ablation threshold in single-crystal Fe is ~0.18 J/cm^2, and ~0.06 J/cm^2 in poly-crystal Fe metal. We can see a clue of the second ablation regime (from figure 5.6) in single crystal Fe when the fluence was raised up to 10 J/cm^2. The second ablation threshold is 1 J/cm^2 from the linearly fitting a few data in the laser fluence region from 10 J/cm^2 to 50 J/cm^2. The ablation threshold difference for the single-crystal and poly-crystal materials should come from the different physical and chemical properties. It will be an interesting topic for future work.

5.5 Potential Applications

Fabricating high aspect ratio holes is a very attractive application for femtosecond laser machining. Femtosecond lasers can be used to cut high-aspect-ratio structures and surface relief gratings (as shown in Figure 5.7 (left)) for photonics applications. Heating of the surrounding area is significantly reduced and consequently the negative aspects associated with heat-affected zones are no longer present. As a result, essentially no melt zones or micro-cracks are formed.

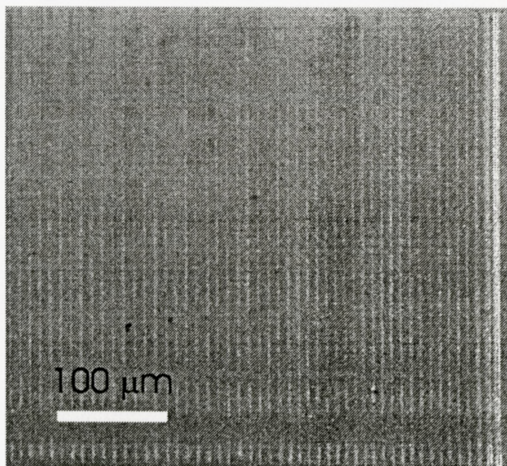

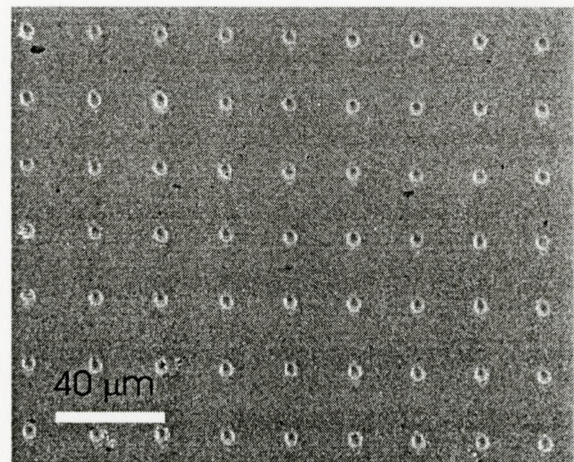

Figure 5.7: (left) Gratings in TiAl , (right) highly reproducible craters array in Fe

Chapter 6. Conclusion

A range of interesting effects observed when using ultrashort pulse laser to process dielectric and metallic materials have been discussed. These results were achieved by a series of ultrashort pulse laser ablation experiments, the first of which addresses the issue of the single-shot and multi-shot irradiation of dielectrics. The second area of investigation is the single-shot work on metallic materials, including single-crystalline Cu, Fe, Al and non-single-crystal Cu, Fe, and Al, etc.

In chapter four on ultrashort pulse laser ablation of dielectric materials, we concluded that the ablation thresholds for BK7 are ~0.64 J/cm^2 and ~0.79 J/cm^2 in fused silica, for single ultrashort laser pulse irradiation (τ=130 fs, λ=790 nm). Also, we believe the ablation threshold of dielectrics in the fs to ps region does not follow a $\tau^{1/2}$; the threshold for 100 fs laser ablation is higher than for ps pulses. However, in order to obtain high quality ablation, fs pulses are definitely better than ps pulses. A clear improvement in the quality of the ablated structures for multi-shot ablation is observed as the pulse width is decreased. Furthermore, ablation threshold fluences in dielectric materials are nearly independent of the wavelength in our experiments. Potential applications in biochemistry and photonics are investigated too. Biochemical sample holders, surface relief gratings and high-aspect ratio trenches have been fabricated with a Ti:sapphire femtosecond laser.

In chapter five on ultrashort pulse laser ablation of metallic materials, we found that the ablated surface morphologies in metals are very different from dielectrics and

semiconductors. Also, some single-crystal metals and poly-crystal metals behave very differently in terms of both surface morphologies and ablation thresholds from the preliminary results on Fe laser ablation. This may be explained by the different properties in these two kinds of materials.

Future detailed work on dielectrics and metals should be done via TEM-based defect analysis. The preliminary TEM result from Cu single crystal that was irradiated by single laser pulses shows few defects in the center region of the ablated crater. Also, from the work of femtosecond laser ablation of semiconductors [30] that was and is being investigated by A. Borowiec, TEM analysis revealed essentially no crystal damage beneath and in the vicinity of the ablation crater. We definitely should extend this technique (TEM) to dielectrics and metals to investigate in detail the femtosecond laser interaction of solid materials.

More work should be done on the comparison of ultrashort laser ablation of single-crystal metals and poly-crystal metals. We have obtained some results from single-crystal Fe and poly-crystal Fe ablation. Al and Cu materials should be explored in the same way too. Surface morphologies of ablated metallic materials by laser pulses with durations from fs to ps should be explored. We have presented the ablation of Cu, Al and Fe with the 120 fs laser pulses at wavelengths 790 nm and 395 nm. We have the capabilities to tune the laser duration from 120 fs to 10 ns; and in the femtosecond case span the wavelength range from 3.0 μm to 300 nm through an optical parametric amplifier and associated nonlinear techniques [30]. Moreover, one can in the future do a lot work on compound metals such as TiAl etc.

In both metallic and dielectric ablation, 10 fs or even shorter duration laser pulses irradiation should be considered. From the publication of M. Lenzner, the ultrashort laser pulses in the 10 fs regime have many advantages [26] in micro-structuring materials compared to 100 fs that was used in our work. Also, the refractive index change induced inside materials by ultrashort laser pulses is another interesting direction. In addition, deep UV femtosecond laser pulse machining dielectrics should be investigated; with 200 nm light or even shorter wavelengths, hopefully 100 nm structures and patterns can be done in dielectrics and metals.

References:

1. G. Timp, editor, "Nanotechnology", Springer-Verlag, (1999).
2. R. W. Waynant, editor, M. N. Ediger, editor, "Electro-optics Handbook", McGraw-Hill, (1994).
3. J. C. Miller, "Laser Ablation - Principles and Applications", Springer-Verlag, (1994).
4. D. Bauerle, editor, "Laser Processing and Chemistry", Springer-Verlag, (2000).
5. W. D. Scharfe and W. Rath, "Lasers for Industrial Applications in Material Processing", Material Science Forum, V301, 253, (1999).
6. A. Niku-Lari, B. L. Mordike, "High Power Lasers", Pergamon Press, (1989).
7. X. Liu, D. Du, and G. Mourou, "Laser Ablation and Micromachining with Ultrashort Laser Pulses", IEEE Journal of Quantum Electronics, V33, 1706, (1997).
8. W. Koechner, "Solid State Laser Engineering", Springer-Verlag, (2000).
9. C. Rulliere, "Femtosecond Laser Pulses: Principles and Experiments", Springer-Verlag, (1998).
10. J. Gowar, "Optical Communication Systems", Prentice Hall, (1993).
11. G. P. Agrawal, "Nonlinear Fiber Optics", Academic Press, (1995).
12. St. Andrews ultrashort pulse laser research group, a website http://www.st-and.ac.uk/~www_pa/group/ultrashort/background/measure/measuret.htm
13. E. E. B. Campbell, "Ultra-short-pulse laser irradiation and ablation of dielectrics", Lasers in Material Science, Trans Tech Publications, 123, (1998).

14. A. Rosenfeld, D. Ashkenasi, H. Varel, M. Wahmer, E.E.B. Campbell, "Time resolved detection of particle removal from dielectrics on femtosecond laser ablation", Applied Surface Science, V127-129, 76, (1998).

15. H. Varel, M. Wahmer, A. Rosenfeld, D. Ashkenasi, E.E.B. Campbell, "Femtosecond laser ablation of sapphire: time-of-flight analysis of ablation plume", Applied Surface Science, V127-129, 128, (1998).

16. H. Varel, D. Ashkenasi, A. Rosenfeld, M. Wahmer, E.E.B. Campbell, "Micromachining of quartz with ultrashort laser pulses", Applied Physics A, V65, 367, (1997).

17. D. Ashkenasi, H. Varel, A. Rosenfeld, F. Noack, E.E.B Campbell, "Pulse-width influence on laser structuring of dielectrics", Nuclear Instruments and Methods in Physics Research B, V122, 359, (1997).

18. D. Ashkenas, H. Varel, A. Rosenfeld, F. Noack, E.E.B Campbell, "Laser processing of sapphire with picosecond and subpicosecond pulses", Applied Surface Science, V120, 65, (1997).

19. H. Varel, D. Ashkenasi, A. Rosenfeld, R, Herrmann, F. Noack, E.E.B. Campbell, "Laser-induced damage in SiO_2 and CaF_2 with picosecond and femtosecond laser pulses", Applied Physics A, V62, 103, (1996).

20. D. Du, X. Liu, G. Korn, J. Squier, G. Mourou: "Laser-induced breakdown by impact ionization in SiO_2 with pulse widths from 7 ns to 150 fs", Applied Physics Letters, V64, 3071, (1994).

21. B. C. Stuart, M. D. Feit, A. M. Rubenchik, B. K. Shore, and M. D. Perry, "Laser-induced damage in dielectrics with nanosecond to subpicosecond pulses", Physical Review Letters, V74, 2248, (1995).

22. M. Lenzner, J. Kruger, S. Sartania, Z. Cheng, Ch. Spielmann, G. Mourou, W. Kautek, F. Krausz, "Femtosecond optical breakdown in dielectrics", Physical Review Letters, V80, 4076, (1998).

23. A. Tien, S. Backus, H. Kapteyn, M. Murnane, G. Mourou, "Short-pulse laser damage in transparent materials as function of pulse duration", Physical Review Letters, V82, 3883, (1999).

24. W. Kautek, J. Kruger, "Laser ablation of dielectrics with pulse durations between 20 fs and 3ps", Applied Physics Letters, V69, 3146, (1996).

25. J. Kruger, W. Kautek, M. Lenzner, S. Sartania, C. Spielmann, F. Krausz, "Laser micromachining of barium aluminum borosilicate glass with pulse durations between 20 fs and 3 ps", Applied Surface Science, V127-129, 892, (1998).

26. M. Lenzner, F. Krausz, J. Kruger, W. Kautek, "Photoablation with sub-10 fs laser pulses", Applied Surface Science, V154-155, (2000).

27. N. Bloembergen, "Laser induced electric breakdown in solids", IEEE Journal of Quantum Electronics, V QE-10, 375, (1974).

28. P. W. Milonni, J. H. Eberly, "Lasers", Wiley-Interscience, (1988).

29. J. Bonse, J.M. Wrobel, J. Kruger, W. Kautek, "Ultrashort-pulse laser ablation of indium phosphide in air". Applied Physics A, V72, 89, (2001).

30. A. Borowiec, M. Eng. thesis "Femtosecond laser ablation of semiconductors", McMaster University, (2000).

31. R. R. Alfano, editor, "The Supercontinuum Laser Source", Springer-Verlag, (1989).

32. C. Kittel, "Introduction to Solid State Physics", Wiley, (1996).

33. P. R. Herman, R. S. Marjoribanks, A. Oettl, K. Chen, I. Konovalov, S. Ness, "Laser shaping of photonic materials: deep-ultraviolet and ultrafast lasers", Applied Surface Science, V154-155, 577, (2000).

34. D. Homoelle, "Infrared photosensitivity in silica glasses exposed to femtosecond laser pulses", Optics Letters, V24, 1311, (1999).

35. K. Chen, J. Ihlemann, P. Simon, I. Baumann, W. Sohker, "Generation of submicorn surface gratings on $LiNbO_3$ by ultrashort UV laser pulses", Applied Physics A, V65, 517, (1997).

36. K. Kawamura, T. Ogawa, N. Sarukura, M. Hirano, H. Hosono, "Fabrication of surface relief gratings on transparent dielectric materials by two-beam holographic method using infrared femtosecond laser pulses", Applied Physics B, V71, 119, (2000).

37. M. Aruna, Y. Murata, H. Nishihara, "Laser-beam direct writing of TiO_2 channels for fabrication of $Ti:LiNbO_3$ waveguides", Japanese Journal of Applied Physics, V31, 1593, (1992).

38. S. Nolte, C. Momma, H. Jacobs, A. Tunnermann, "Ablation of metals by ultrashort laser pulses", Journal of Optical Society of America B. V14, 2716, (1997).

39. X. Zhu, A. Y. Naumov, D. M. Villeneuve, P. B. Corkum, "Influence of laser parameters and material properties on micro drilling with femtosecond laser pulse", Applied Physics A, V69, 367, (1999).

40. P. S. Bands, M. D. Feit, A. M. Rubenchik, B. C. Stuart, M. D. Perry, "Material effects in ultra-short pulse laser drilling of metals", Applied Physics A, V69, 377, (1999).

41. S. Preuss, A. Demchuk, M. Stuke, "Sub-picosecond UV laser ablation of metals", Applied Physics A, V72, 45, (2001).

42. K. Furusawa, K. Takahashi, H. Kumagai, K. Midorikawa, M. Obara, "Ablation characteristics of Au, Ag and Cu metals using a femtosecond Ti:sapphire laser", Applied Physics A, V69, 359, (1999).

43. P. Simon, J. Ihlemann, "Machining of submicron structures on metals and semiconductors by ultrashort UV-laser pulses", Applied Physics A, V63, 505, (1996).

44. H. Strehlow, "Shockwaves in laser-pulse-irradiated metals", Applied Physics A, V72, 45, (2001).